UNIVERSITY OF OKLAHOMA

GRADUATE COLLEGE

UNDERSTANDING THE FEATURES AND MECHANISMS OF THE GREAT

PLAINS LOW-LEVEL JET IN CMIP5 MODELS

A THESIS

SUBMITTED TO THE GRADUATE FACULTY

in partial fulfillment of the requirements for the

Degree of

MASTER OF SCIENCE IN METEOROLOGY

By

JAMES DANCO
Norman, Oklahoma
2016

UNDERSTANDING THE FEATURES AND MECHANISMS OF THE GREAT
PLAINS LOW-LEVEL JET IN CMIP5 MODELS

A THESIS APPROVED FOR THE
SCHOOL OF METEOROLOGY

BY

_____
Dr. Elinor Martin, Chair

_____
Dr. Jason Furtado

_____
Dr. Susan Postawko

Acknowledgements

Table of Contents

List of Tables

List of Figures

Abstract

The Great Plains low-level jet (GPLLJ) is an important driver of precipitation and severe weather outbreaks over the U.S. Great Plains during the spring and summer. Therefore, it is extremely important that features of the GPLLJ, including its atmospheric and oceanic mechanisms, are understood and simulated accurately by global climate models so Great Plains precipitation can be predicted reliably in the future. This study examines the features of the GPLLJ and the mechanisms relating it to the El Niño Southern Oscillation (ENSO) in reanalyzes and global climate models, to aid near- and long-term predictions and projections of Great Plains weather and climate. Sea surface temperature data, four reanalyzes, and an ensemble of 42 historical simulations from phase 5 of the Coupled Model Intercomparison Project (CMIP5) are used. This makes this study the first of its kind to examine the ability of the entire suite of CMIP5 models to represent the observed features of the GPLLJ and its relationship with ENSO. Biases in the CMIP5 model simulation of the climatology of the GPLLJ are identified, including a GPLLJ that is too weak, extends too late in the summer, and peaks too low in the troposphere. Noting these biases, the accuracy of the ENSO - GPLLJ relationship in the CMIP5 models is investigated. As in previous studies, observations and reanalysis show that winter ENSO has a significant negative correlation with the GPLLJ in the following spring and a significant positive correlation with the GPLLJ in the following summer. This study illustrates that the influence of ENSO on the GPLLJ is mainly on the frequency, not intensity, of GPLLJ events in the spring, while both the frequency and intensity of GPLLJ events are affected in the summer. However, although the majority of CMIP5 historical simulations (82 out of 131 ensemble members) exhibit the observed

significant negative ENSO - GPLLJ correlations in the spring, nearly all of them (129 out of 131 ensemble members) fail to simulate the significant positive correlation in the summer. The ability of the models to simulate the ENSO - GPLLJ relationship is attributed to the strength of simulated ENSO events and the associated effects on geopotential heights and atmospheric circulation. These results have implications for the predictability of climate in the Great Plains and suggest that the variability of the GPLLJ will not be reliably captured in future climate simulations if the magnitude of ENSO events and their impacts are not well represented.

Chapter 1: Introduction

During the months of March through September, the Great Plains of the United States frequently experiences a nocturnal southerly flow of air from just above the surface to approximately 850 hPa, known as the Great Plains low-level jet (GPLLJ) (Higgins et al. 1997). As shown in Fig. 1, the GPLLJ is strongest from Texas to Kansas, where a mean southerly flow at 850-hPa is evident from March through September, to the west of 98°W. To the east of 98°W and to the north of 32°N, the winds turn southwesterly. This phenomenon significantly increases nocturnal convective precipitation over the Great Plains by transporting moisture from the Gulf of Mexico (GOM) and providing low-level convergence at its northern edges, resulting in the production of mesoscale convective systems (Stensrud 1996; Higgins et al. 1997; Weaver and Nigam 2008; Weaver et al. 2009). As shown by Weaver et al. (2009), a stronger GPLLJ can result in precipitation extremes, with a higher likelihood of drought conditions at the entrance region (southeastern U.S.) and flood conditions at the exit region (central U.S.). The devastating 1993 floods and 1988 drought in the Midwest have been attributed to variations in the GPLLJ (Trenberth and Guillemot 1996; Arritt et al. 1997). It has also been found that both the strength and northward extent of the springtime GPLLJ significantly increased from 1979-2012, associated with substantial increases in the frequency and intensity of precipitation in the Northern Plains and decreases in precipitation throughout the Southern Plains (Barandiaran et al. 2013).

In addition to effects on precipitation, a more intense GPLLJ results in conditions more conducive to tornado outbreaks across the U.S., through increased southerly moisture transport from the GOM and greater vertical wind shear (Lee et al. 2013). The

GPLLJ is also important for seed dispersion and the migration of birds and insects, which affects agriculture and anyone influenced by the influx of pests and diseases (Stensrud 1996). Clearly the GPLLJ has a large impact on the Great Plains, so developing accurate predictions and projections of the timing, location, and intensity of the GPLLJ is vital for the economy, agriculture, and overall livelihood of the people living there. Understanding the mechanisms that are responsible for controlling the variations in the GPLLJ, as well as the ability of global climate models (GCMs) to simulate them, is crucial for improving predictions and projections.
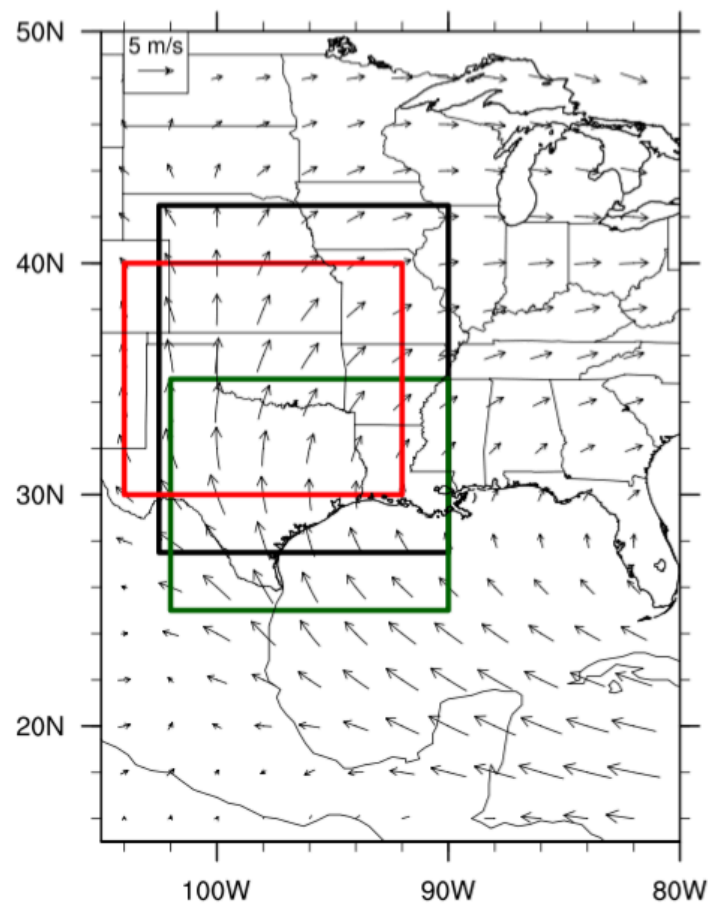
Figure 1: Mean 850-hPa wind vectors in the 20CR from March through September. Boxes illustrate the regions used for the MAM GPLLJ index (green), JAS GPLLJ index (red), and annual GPLLJ index (black).

2

Theories have been proposed explaining the formation, timing, and location of the GPLLJ. Blackadar (1957) proposed that low-level jet (LLJ) formation occurs at night due to a sharp reduction in friction at sunset, which results from a stabilization of the planetary boundary layer (PBL) by radiative cooling at the land surface. A theory by Holton (1967) explains the common occurrence of a LLJ over the Great Plains. It suggests that the GPLLJ is driven by the diurnal oscillation of the pressure gradient force, resulting from the alternative heating and cooling over the sloping terrain of the Rocky Mountains. According to Jiang et al. (2007), the diurnal cycle and amplitude of the GPLLJ can be attributed to a combination of these two mechanisms proposed by Blackadar (1957) and Holton (1967). In addition, Wexler (1961) proposed that the GPLLJ results from a westward extension of the Bermuda high, and it is shaped by the orographic configuration in North America, especially the Rocky Mountain Plateau which serves as a western barrier for the GPLLJ. Leeside cyclogenesis (or leeside troughing) on the eastern slopes of the Rockies has also been shown to play a role in the development of the GPLLJ by increasing the lower-tropospheric pressure gradient over the central U.S. (Uccellini 1980).

Observations have shown that one important influence on the intensity of the GPLLJ are sea surface temperature (SST) anomalies in the equatorial Pacific Ocean, associated with the El Niño - Southern Oscillation (ENSO). Muñoz and Enfield (2011) discovered that colder SSTs in the Niño 3.4 region (5°S-5°N, 170°W-120°W) often result in a stronger GPLLJ in the spring, while other studies have found that a warm equatorial Pacific strengthens the GPLLJ in the summer (Schubert et al. 2004; Weaver et al. 2009). These results have significant implications for the predictability of the GPLLJ because

they demonstrate that if the state of ENSO can be known in advance, the intensity of the GPLLJ can be predicted.

Krishnamurthy et al. (2015) found that one of the mechanisms that plays a major role in this shift from negative to positive correlations between ENSO and the GPLLJ from the spring to summer is the Caribbean low-level jet (CLLJ). Studies have shown a positive correlation between the CLLJ and GPLLJ (Cook and Vizy 2010; Martin and Schumacher 2011). Observations indicate wintertime La Niña induces high sea level pressure (SLP) anomalies over the Intra-Americas Sea (IAS) the following spring through changes in the Walker and Hadley circulation. This leads to a strong CLLJ, which drives a stronger GPLLJ. In the summer, however, an El Niño is associated with low SLP anomalies in the tropical Pacific and high SLP anomalies in the tropical Atlantic. This strong SLP gradient results in a stronger CLLJ, which again leads to a stronger GPLLJ. In addition to this tropical link, it has been hypothesized that ENSO can affect the GPLLJ through an extratropical wave train from the tropical west Pacific into North America (Krishnamurthy et al. 2015).

The impact of ENSO on the GPLLJ varies depending on the spatial pattern of SSTs in the tropical Pacific. Lee et al. (2013) found that in April and May, cold SST anomalies in the Niño 4 region (5°S-5°N, 160°E-150°W) and warm SST anomalies in the Niño 1+2 region (0°-10°S, 90°-80°W) work together to result in increased moisture transport from the GOM, which could imply a stronger GPLLJ. Another recent study discovered a similar pattern in the summer, with a Central Pacific (CP) El Niño weakening the GPLLJ and an East Pacific (EP) El Niño strengthening it (Liang et al. 2015).

4

The variability of the GPLLJ is affected by many other teleconnections besides ENSO. Harding and Snyder (2015) found that the GPLLJ is enhanced by a negative phase of the Pacific-North American teleconnection pattern (PNA), which is associated with higher geopotential heights in the central north Pacific and the southeastern U.S. and lower heights near the west coast of North America. This enhancement is due to a strengthening of the pressure gradient across the central U.S. Muñoz and Enfield (2011) discovered a significant negative correlation between the Pacific Decadal Oscillation (PDO) and the GPLLJ in the spring, and Weaver and Nigam (2008) discovered a link between GPLLJ variability and North Atlantic Oscillation (NAO) variability in the summer.

It is known that GCMs are unable to represent some of the features of the GPLLJ in their historical simulations. Sheffield et al. (2013) compared the GPLLJ simulation in eight models from phase 5 of the Coupled Model Intercomparison Project (CMIP5) to the NCEP-NCAR reanalysis. The models place the peak of the GPLLJ at about 925 hPa, while the reanalysis has it at 850 hPa. The simulated GPLLJ also extends farther north compared to the reanalysis, and the models extend the peak of the GPLLJ into late July while the reanalysis weakens it by early July (Sheffield et al. 2013). Cook et al. (2008) also discovered that the prior generation of GCM's simulate a GPLLJ that is too weak in their twentieth-century simulations.

GCM's also struggle with simulating the strength and structure of ENSO, which is hypothesized to have an effect on their ability to represent the correct influence of ENSO on the GPLLJ. Kim and Yu (2012) evaluated 20 CMIP5 models and found that only nine of them can simulate realistically strong EP and CP ENSO intensities in their

preindustrial simulations, with the models particularly struggling to represent EP ENSO intensity. Furthermore, a narrow bias in meridional width of SST anomalies associated with ENSO has been found in CMIP5 models (Zhang and Jin 2012). An underestimate of ENSO asymmetry, the tendency for the strongest El Niños to be stronger than the strongest La Niñas, is a problem in CMIP5 models as well (Zhang and Sun 2014). Krishnamurthy et al. (2015) found that the GFDL FLOR coupled climate model simulates too much ENSO variability and inaccurate phase locking, which results in a negative ENSO - GPLLJ correlation in both the spring and summer seasons, in contrast to observations.

Despite these errors in GCM representation of the features and mechanisms of the GPLLJ, projected changes in the strength of the GPLLJ have been examined. Cook et al. (2008) discovered that models from phase 3 of the Coupled Model Intercomparison Project (CMIP3) project a more intense GPLLJ in April-May-June over the course of the twenty-first century, which enhances precipitation by 20-40% in the upper Midwest. This continues the observed increase in the strength of the GPLLJ discovered by Barandiaran et al. (2013). Similarly, Harding and Snyder (2014) found that two CMIP5 models under the Representative Concentration Pathway (RCP) 8.5 scenario project a stronger GPLLJ during April-July by 2090-2099, which results in more frequent extreme rainfall events and increased total precipitation over the north-central U.S. However, the models slightly weaken the GPLLJ during August-September, which causes increases in drought in this region (Harding and Snyder 2014).

These future changes in the intensity and timing of the GPLLJ, and thus in precipitation and severe weather over the Great Plains, cannot be accurately projected if

the features and mechanisms of the GPLLJ are not understood and simulated correctly by GCMs. Therefore, an understanding of the GPLLJ and the mechanisms affecting it is crucial, as is the ability of GCMs to represent it, in order to improve near- and long-term predictions and projections of Great Plains weather and climate. While some studies have examined the ability of GCMs to simulate the climatology of the GPLLJ, little focus has been given on their ability to represent its variability at a process-level. This study investigates the features and mechanisms of the GPLLJ in CMIP5 models, with a focus on the effects of ENSO on the GPLLJ. Factors that influence the models' ability to capture GPLLJ features and mechanisms are also examined.

Chapter 2 includes a description of the observed data, reanalyzes, and model output, as well as a discussion of the methodology. Chapter 3 examines the climatology of the GPLLJ in the CMIP5 models and compares it to the reanalyzes. Chapter 4 discusses the relationship between ENSO and the GPLLJ in observations and the ability of the CMIP5 models to simulate it. Chapter 5 demonstrates factors affecting the models' ability to represent the accurate ENSO – GPLLJ relationship. Chapter 6 summarizes the findings of the study while establishing questions that could be the subject of future research.

Chapter 2: Data and Methods

The GPLLJ climatology analysis uses monthly meridional wind data over 1900-2005 from 42 coupled atmosphere-ocean general circulation models (AOGCM's), with 131 individual ensemble members coordinated under CMIP5 (Table 1). However, further analysis involving zonal wind, SLP, and geopotential heights, only uses 31 of the original 42 models due to data availability issues. The model data was downloaded using the Program for Climate Model Diagnosis and Intercomparison (PCMDI) web portal (http://pcmdi9.llnl.gov/) and the German Climate Computing Center (DKRZ) web portal (http://esgf-data.dkrz.de/). The experimental design used is a historical simulation of twentieth-century climate. The model output is at a wide range of horizontal resolutions (Table 1), so to facilitate comparison, their output was interpolated to a common 2° by 2° latitude-longitude grid using bilinear interpolation. Since many of the models had multiple ensemble members, model averages were obtained by averaging over all ensemble members for each model first, to avoid a bias toward the models with many ensemble members. This CMIP5 model mean will be referred to as the model mean throughout this study.

Model number	Model name	Modeling center	Number of ensemble members	Horizontal resolution (° latitude by ° longitude)	Reference	Subset
1	BCC-CSM1.1	Beijing Climate Center, China Meteorological Administration	3	2.8125 x 2.8125	Xin et al. 2012	
2	BCC-CSM1.1-M	Beijing Climate Center, China Meteorological Administration	3	1.125 x 1.125	Xin et al. 2012	
3	CanESM2	Canadian Centre for Climate Modeling and Analysis	5	2.8125 x 2.8125	Arora et al. 2011	
4	CCSM4	National Center for Atmospheric Research	6	0.9375 x 1.25	Gent et al. 2011	
5	CESM1-BGC	Community Earth System Model Contributors	1	0.9375 x 1.25	Long et al. 2013	
6	CESM1-CAM5	Community Earth System Model Contributors	3	0.9375 x 1.25	Meehl et al. 2013	
7	CESM1-FASTCHEM	Community Earth System Model Contributors	3	0.9375 x 1.25	Perez et al. 2014	
8	CESM1-WACCM	Community Earth System Model Contributors	1	1.875 x 2.5	Marsh et al. 2013	
9	CMCC-CESM	Centro Euro-Mediterraneo per I Cambiamenti Climatici	1	3.75 x 3.75	Perez et al. 2014	X
10	CMCC-CM	Centro Euro-Mediterraneo per I Cambiamenti Climatici	1	0.75 x 0.75	Perez et al. 2014	X
11	CMCC-CMS +	Centro Euro-Mediterraneo per I Cambiamenti Climatici	1	1.875 x 1.875	Perez et al. 2014	X
12	CNRM-CM5	Centre National de Recherches Météorologiques / Centre Européen de Recherche et Formation Avancée en Calcul Scientifique	10	1.40625 x 1.40625	Voldoire et al. 2013	X
13	CNRM-CM5-2 + +	Centre National de Recherches Météorologiques / Centre Européen de Recherche et Formation Avancée en Calcul Scientifique	1	1.40625 x 1.40625	Voldoire et al. 2013	X
14	CSIRO-Mk3L-1-2	Commonwealth Scientific and Industrial Research Organization in collaboration with Queensland Climate Change Centre of Excellence	3	3.2 x 5.625	Phipps et al. 2011	
15	FGOALS-g2	LASG, Institute of Atmospheric Physics, Chinese Academy of Sciences and CESS, Tsinghua University	5	3.0 x 2.8125	Li et al. 2013	X
16	FGOALS-s2 +	LASG, Institute of Atmospheric Physics, Chinese Academy of Sciences	2	1.7 x 2.8125	Bao et al. 2012	X
17	GFDL-CM2.1 + *	NOAA Geophysical Fluid Dynamics Laboratory	10	2.0 x 2.5	Delworth et al. 2006	X
18	GFDL-CM3	NOAA Geophysical Fluid Dynamics Laboratory	5	2.0 x 2.5	Donner et al. 2011	X
19	GFDL-ESM2G	NOAA Geophysical Fluid Dynamics Laboratory	1	2.0 x 2.5	Donner et al. 2011	X
20	GFDL-ESM2M + *	NOAA Geophysical Fluid Dynamics Laboratory	1	2.0 x 2.5	Donner et al. 2011	X
21	GISS-E2-H *	NASA Goddard Institute for Space Studies	5	2.0 x 2.5	Kim et al. 2012	X
22	GISS-E2-H-CC *	NASA Goddard Institute for Space Studies	1	2.0 x 2.5	Kim et al. 2012	X
23	GISS-E2-R +	NASA Goddard Institute for Space Studies	3	2.0 x 2.5	Kim et al. 2012	X

#	Model	Institution		Resolution	Reference	
24	GISS-E2-R-CC +	NASA Goddard Institute for Space Studies	1	2.0 x 2.5	Kim et al. 2012	X
25	HadCM3	Met Office Hadley Centre	10	2.5 x 3.75	Collins et al. 2001	X
26	HADGEM2-AO +	National Institute of Meteorological Research/Korea Meteorological Administration	1	1.25 x 1.875	Baek et al. 2013	X
27	HADGEM2-CC	Met Office Hadley Centre	1	1.25 x 1.875	Jones et al. 2011	X
28	HADGEM2-ES	Met Office Hadley Centre	5	1.25 x 1.875	Jones et al. 2011	X
29	INM-CM4.0 * *	Institute for Numerical Mathematics	1	1.5 x 2.0	Volodin et al. 2010	X
30	IPSL-CM5A-LR	Institut Pierre-Simon Laplace	6	1.875 x 3.75	Dufresne et al. 2013	X
31	IPSL-CM5A-MR	Institut Pierre-Simon Laplace	3	1.25 x 2.5	Dufresne et al. 2013	X
32	IPSL-CM5B-LR *	Institut Pierre-Simon Laplace	1	1.875 x 3.75	Dufresne et al. 2013	X
33	MIROC5	Atmosphere and Ocean Research Institute (The University of Tokyo), National Institute for Environmental Studies, and Japan Agency for Marine-Earth Science and Technology	5	1.40625 x 1.40625	Watanabe et al. 2010	X
34	MIROC-ESM *	Japan Agency for Marine-Earth Science and Technology, Atmosphere and Ocean Research Institute (The University of Tokyo), and National Institute for Environmental Studies	3	2.8125 x 2.8125	Watanabe et al. 2010	X
35	MIROC-ESM-CHEM *	Japan Agency for Marine-Earth Science and Technology, Atmosphere and Ocean Research Institute (The University of Tokyo), and National Institute for Environmental Studies	1	2.8125 x 2.8125	Watanabe et al. 2010	X
36	MPI-ESM-LR	Max-Planck-Institut für Meteorologie (Max Planck Institute for Meteorology)	3	1.875 x 1.875	Zanchettin et al. 2013	X
37	MPI-ESM-MR	Max-Planck-Institut für Meteorologie (Max Planck Institute for Meteorology)	3	1.875 x 1.875	Zanchettin et al. 2013	X
38	MPI-ESM-P *	Max-Planck-Institut für Meteorologie (Max Planck Institute for Meteorology)	2	1.875 x 1.875	Zanchettin et al. 2013	X
39	MRI-CGCM3	Meteorological Research Institute	5	1.125 x 1.125	Yukimoto et al. 2012	X
40	MRI-ESM1	Meteorological Research Institute	1	1.125 x 1.125	Adachi et al. 2013	X
41	NorESM1-M	Norwegian Climate Centre	3	1.875 x 2.5	Bentsen et al. 2013	
42	NorESM1-ME	Norwegian Climate Centre	1	1.875 x 2.5	Bentsen et al. 2013	

Table 1: List of CMIP5 models included in the analysis and their attributes. The last column is marked with an "X" if the model is included in the subset of 31 models used for the additional analysis. The five best (worst) spring models, defined as the five models out of the subset with the strongest (weakest) negative DJF ENSO – MAM GPLLJ correlation, are indicated by + (*). The five best (worst) summer models, defined as the five models out of the subset with the strongest positive (negative) DJF ENSO – JAS GPLLJ correlation, are indicated by + (*).

The model output is compared to monthly data from four reanalyzes: the Twentieth Century Reanalysis version 2c (20CR: resolution of 2° x 2°, 1900-2014, Compo et al. 2011), ECMWF twentieth century reanalysis (ERA20C: resolution of 1° x 1°, 1900-2010, Poli et al. 2016), ECMWF interim reanalysis (ERA-Interim: resolution of 0.75° x 0.75°, 1979-2015, Simmons et al. 2014), and NCEP Climate Forecast System Reanalysis (CFSR: resolution of 0.5° x 0.5°, 1979-2009, Saha et al. 2010). Six-hourly meridional wind data from ERA-Interim and three CMIP5 models (CNRM-CM5, FGOALS-g2, and MIROC-ESM) is used in Chapter 4, Section c. Only three models were used because of limited access to CMIP5 six-hourly wind data.

Monthly SST observations from 1900-2015 are from the Hadley Centre Global Sea Ice and Sea Surface Temperature dataset (HadISST1: resolution of 1° x 1°, Rayner et al. 2003). The monthly Extended Reconstructed Sea Surface Temperature dataset (ERSST: resolution of 2° x 2°, Huang et al. 2015) is also used in Chapter 5, Section b. The resolution of the reanalyzes/observations differs from one another and from the models, but unlike the models, no regridding was done. This is because the resolutions of the reanalyzes/observations do not vary as much as they do in the models, and the regions examined for SST and wind data are large enough that it was determined that interpolation to a common resolution would not have a significant impact on the results of this study.

The definition of the GPLLJ index is the same as that used by Harding and Snyder (2015); the area-averaged 850-hPa meridional wind speed over 27.5°-42.5°N, 102.5°-90°W (Fig. 1; black box). As shown by Krishnamurthy et al. (2015), the relationship between the GPLLJ and ENSO experiences a seasonal shift from the spring to the summer, so this study will also examine the GPLLJ in both seasons. Cook et al. (2008) demonstrate that the GPLLJ is not stationary in space, shifting north from the spring to the summer, so two different regions are used for the spring and summer GPLLJ. These regions of interest were chosen based on where the GPLLJ is strongest in the 20CR. The March-April-May (MAM) GPLLJ index is defined over 25°-35°N, 102°-90°W (Fig. 1; green box), and the July-August-September (JAS) GPLLJ index is defined over 30°-40°N, 104°-92°W (Fig. 1; red box).

ENSO is measured with the Oceanic Niño Index (ONI), defined as the three-month running mean of SST anomalies in the Niño 3.4 region using a base period of 1971-2000 (Eichler and Higgins 2006). Weak, moderate, and strong El Niño (La Niña) events are defined as SST anomalies ≥ 1 and < 1.5, ≥ 1.5 and < 2, and ≥ 2 standard deviations above (below) the mean, respectively. In the observations, there are a total of eight weak, nine moderate, and two strong El Niño events, respectively, and there are a total of seven weak, seven moderate, and one strong La Niña event, respectively. There are an average of 9.2 weak, 4.7 moderate, and 2.9 strong El Niño events in each model, respectively, and there are an average of 10.0 weak, 4.6 moderate, and 1.7 strong La Niña events in each model, respectively. Standard deviation is used for the threshold in order to facilitate comparison between models that may have differing magnitudes of ENSO variability.

Throughout this study, statistical significance is evaluated using two-tailed t-tests, except in Section 3c when a 95% confidence interval of bootstrapped errors is used to determine significance. The effective degrees of freedom is calculated using n-2, where n is the number of years/seasons in the given sample. Correlations are computed using the Pearson sample linear cross-correlation. All data is detrended before correlation analysis.

Chapter 3: GPLLJ Climatology

Section 3a: Annual Cycle

The annual cycle of the GPLLJ index from the 20CR, ERA20C, ERA-Interim, CFSR, and CMIP5 model mean is shown in Fig. 2a. All four reanalyzes agree on the timing of the GPLLJ, with the peak in June, consistent with previous studies (Cook et al. 2008; Sheffield et al. 2013). The model mean extends its peak from June through August while the reanalyzes sharply weaken it after June. This agrees with the results from Sheffield et al. (2013) which only used eight CMIP5 models. The GPLLJ in the models is too weak throughout the year, except during JAS, consistent with the findings from Cook et al. (2008). In fact, the model mean is greater than one standard deviation below the reanalysis mean during all months of the year except from June through September (Fig. 2a). In order to examine the effects, if any, of using different years for the reanalyzes and models, Fig. 2b shows the annual cycle of the GPLLJ over just the years that overlap between all the reanalyzes and the models (1979-2005). Overall, the results are similar to Fig. 2a, except that the model mean is closer to the reanalysis mean in April and May, and the strength of the GPLLJ in the 20CR is closer to the other reanalyzes.
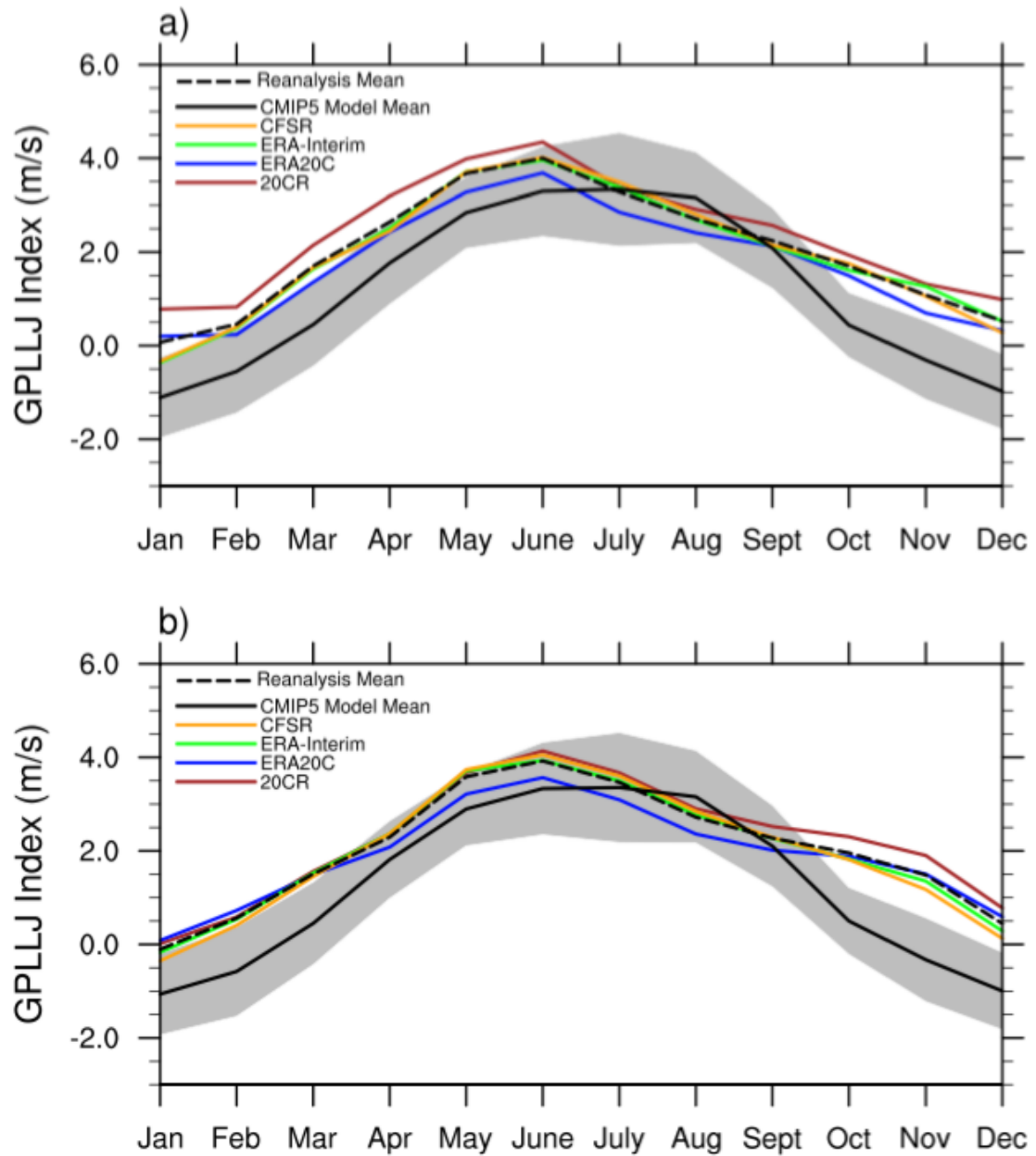
Figure 2: Annual cycle of the GPLLJ index over all years (a) and over just 1979-2005 (b) for the 20CR, ERA20C, ERA-Interim, CFSR, reanalysis mean, and CMIP5 model mean. The gray shading indicates +/- one standard deviation above and below the model mean.

Section 3b: Diurnal Cycle

The diurnal cycle of the MAM GPLLJ index in three CMIP5 models is compared

to the ERA-Interim in Fig. 3a. The GPLLJ is strongest in the ERA-Interim at 06Z,

15

consistent with previous studies (Higgins et al. 1997; Jiang et al. 2007; Pu and Dickinson 2014). Overall, the diurnal cycle in the models compares well to the reanalysis, as all three capture the observed peak in the MAM GPLLJ at 06Z. However, the minimum strength of the MAM GPLLJ in the ERA-Interim occurs at 00Z, while in the CNRM-CM5 and MIROC-ESM the GPLLJ is weakest at 12Z. Consistent with the results from Section 3a, each of the three models also simulates a MAM GPLLJ that is too weak at all times of day (with the exception of the CNRM-CM5 at 00Z) (Fig. 3a). As in MAM, the JAS GPLLJ index peaks at 06Z in all three models and in the ERA-Interim, but the intensity of the JAS GPLLJ is more comparable between the models and the reanalysis than in MAM (Fig. 3b). Furthermore, it is clear that the GPLLJ in the models and reanalysis exhibits a stronger diurnal variation in JAS than in MAM. This could be due to enhanced daytime solar heating in JAS resulting in a greater diurnal oscillation in pressure gradient force or in a greater change in stability from day to night, theories for GPLLJ formation proposed by Holton (1967) and Blackadar (1957), respectively.
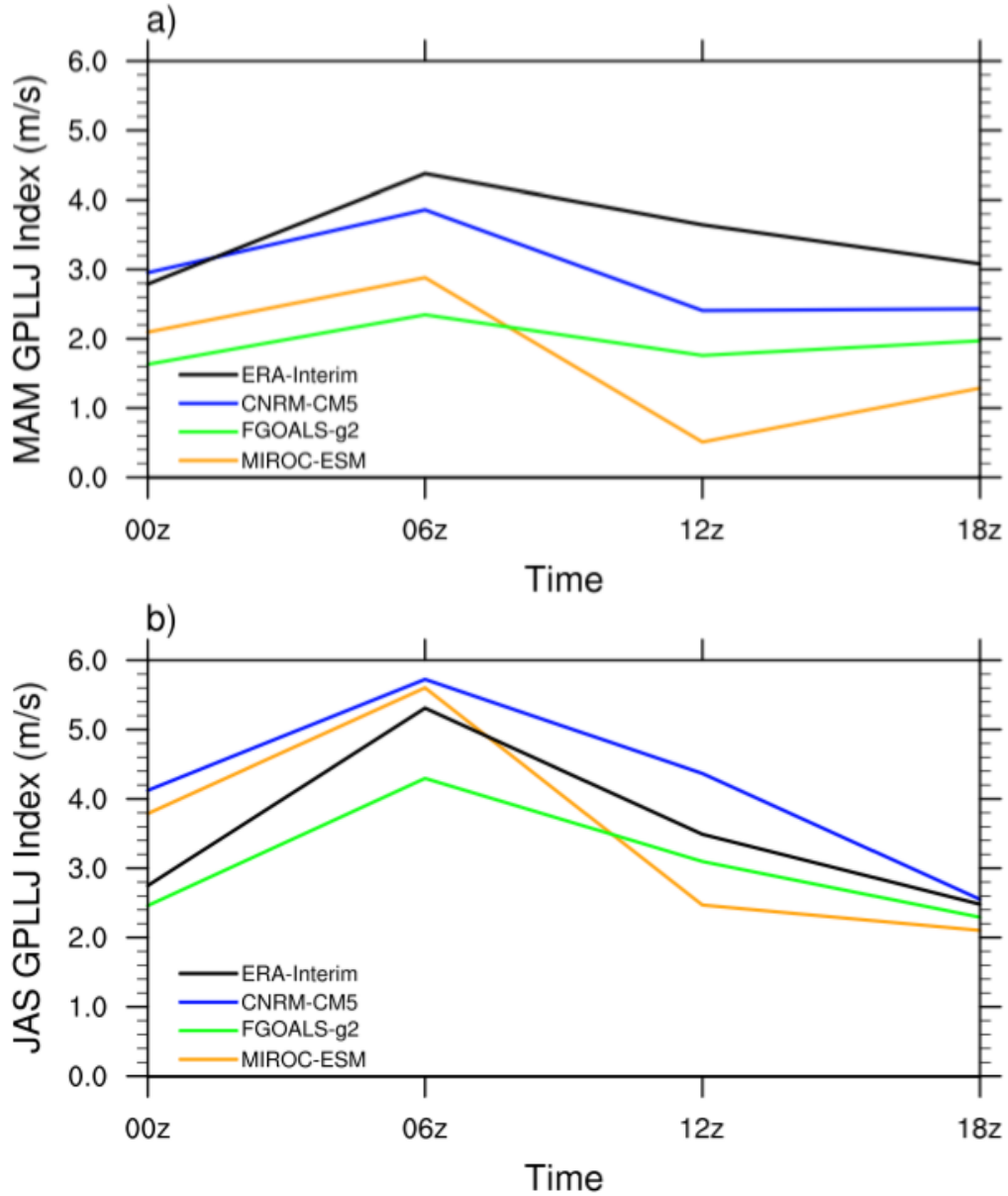
Figure 3: Diurnal cycle of the MAM (a) and JAS (b) GPLLJ index in the ERA-Interim, CNRM-CM5, FGOALS-g2, and MIROC-ESM.

Section 3c: Intensity

As discussed in Section 3a, the model mean simulates a GPLLJ that is weaker than reanalysis. To determine the robustness of this model mean result, a statistical analysis is performed to determine the ability of each CMIP5 model to simulate the strength of the GPLLJ using the difference between the modeled and observed 850-hPa

17

meridional wind at each grid point over the MAM and JAS GPLLJ regions. The 20CR is used for the observed GPLLJ because it covers similar years to the CMIP5 models, and the strength of the GPLLJ in the 20CR agrees very closely with the ERA-Interim and CFSR when only examining the years they have in common, unlike the ERA20C (Fig. 2b). These differences (errors) are bootstrapped 1000 times for each model, and a 95% confidence interval is evaluated for these differences to determine if each model error is significant.

As shown in Fig. 4, the MAM model mean GPLLJ is significantly weaker than the 20CR, as expected from Fig. 2. All models simulate a GPLLJ that is too weak, and 25 out of the 42 models (~60%) have a MAM GPLLJ that is significantly weaker than the 20CR (Table A1). The median, quartiles, and outliers for every model are less than zero, with the median errors ranging from approximately -0.5 m/s to -2.5 m/s (Fig. 4).

In addition, the errors in model GPLLJ strength from the same modeling group are often similar. For example, the boxplots for all four of the Hadley Centre models (indices 25-28) are clustered together, and they each have some of the smallest errors of models examined in this study (Fig. 4). This pattern often holds for the variance in the GPLLJ as well. Both the MIROC-ESM models (indices 34-35), for instance, share very similar interquartile ranges (IQRs), which are on the high end of all the models (Fig. 4). This is important because it indicates that the similarities in physics between models from the same modeling group play a large role in their ability to accurately simulate the strength of the GPLLJ. However, this relationship does not hold for every modeling group, which indicates that other factors, such as differences in model resolution and carbon cycling, can be important in the simulation of the GPLLJ as well.
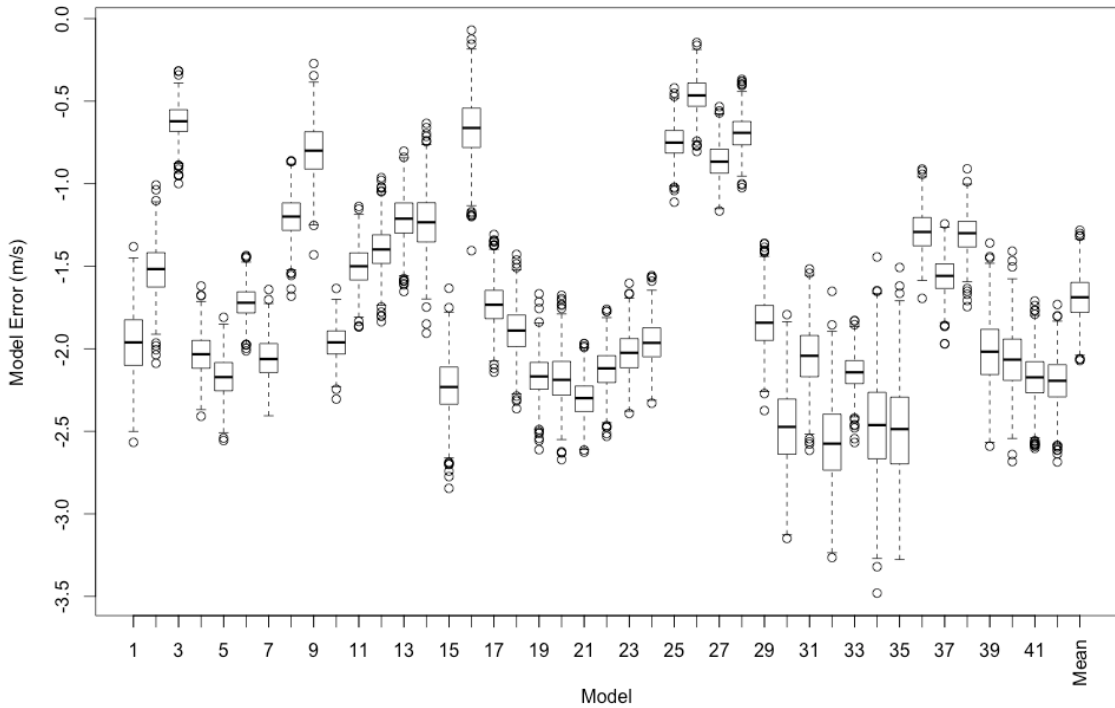
Figure 4: Boxplots of the bootstrapped differences (R=1000) between the MAM GPLLJ in 42 CMIP5 models and 20CR. The index for each model shown on the horizontal axis is given in Table 1.

It is interesting to compare the MAM GPLLJ intensity results with JAS, when the reanalysis and model mean are more similar (as seen in Fig. 2), the results of which are presented in Fig. 5. The model mean JAS GPLLJ is not significantly different from the 20CR and the GPLLJ magnitude differences are much less than in MAM. Only six of the 42 models (~14%) have a GPLLJ that is significantly weaker than the reanalysis, while three models (~7%) have a significantly stronger GPLLJ (Table A2). Fig. 5 shows that the median bootstrapped error is greater than zero for 14 (one-third) of the models, and the median errors range from approximately -2 m/s to 2 m/s, in contrast to MAM when all the models have a GPLLJ that is too weak. These results indicate much better model performance in simulating the strength of the GPLLJ in JAS compared to MAM.

19

However, it should be noted that this is only because the models extend the peak of the GPLLJ too late in the summer, so it appears to be the right answer for the wrong reason.

As in MAM, most models from the same modeling group have very comparable amounts of error and variance in JAS. For example, all four GISS models (indices 21-24) have similar error magnitudes and amounts of variance (Fig. 5). The models often retain these characteristics from the spring to the summer. For instance, the two MIROC-ESM models (indices 34-35) continue to have high amounts of variance. Furthermore, the three HadGEM2 models (indices 26-28) are among the models that simulate the JAS GPLLJ the strongest, as they were in MAM, but the HadCM3 model (index 25) is now substantially weaker (Fig. 5).
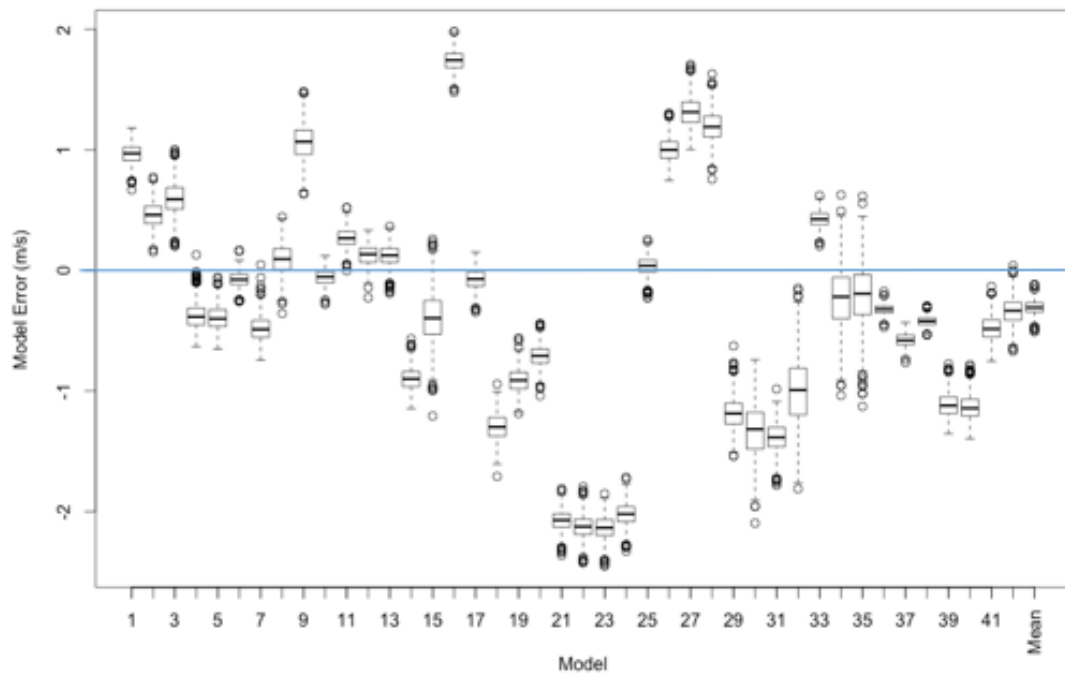
Figure 5: Same as Fig. 4, but for JAS.

20

The pressure gradient across the central U.S. has been shown to play a major role in the strength of the GPLLJ (Harding and Snyder 2015). This means accurate simulation of this pressure gradient is crucial for the models' ability to represent the observed GPLLJ intensity. From Fig. 6, it is apparent that the five CMIP5 models with the weakest MAM GPLLJ (the "weakest spring models"), exhibit a weaker gradient in correlation between the GPLLJ and SLP over the Great Plains than the five models with the strongest MAM GPLLJ (the "strongest spring models"). Therefore, a pressure gradient that is too weak in the CMIP5 models could be contributing to their inability to capture the observed GPLLJ intensity in MAM. This is further confirmed by the weaker mean MAM SLP gradient over the central U.S. in the "weakest spring models" compared to the "strongest spring models" (Fig. B1). Similarly, the five models with the weakest JAS GPLLJ (the "weakest summer models") simulate a weaker mean JAS SLP gradient across the central U.S. than the five models with the strongest JAS GPLLJ (the "strongest summer models"), indicating that this may also at least partially explain why some models simulate the GPLLJ too strong or too weak in JAS (Fig. B2). However, other factors could be having an effect as well, including differences in model resolution, in representation of orographic features, or in simulation of other known influences on the GPLLJ such as the CLLJ, PDO, or NAO (Weaver and Nigam 2008; Cook and Vizy 2010; Martin and Schumacher 2011; Muñoz and Enfield 2011).
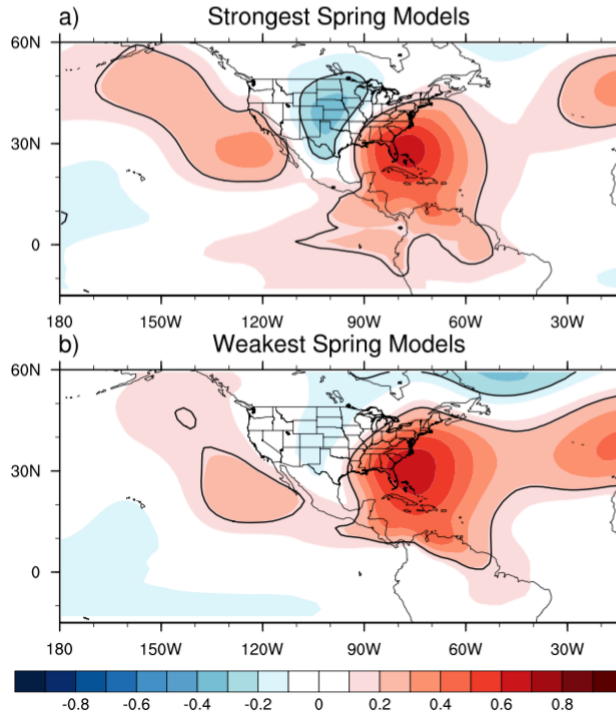
Figure 6: Instantaneous cross-correlation between anomalies of the GPLLJ and SLP in MAM in the five models with the strongest MAM GPLLJ (a) and the five models with the weakest MAM GPLLJ (b). All correlations within the bolded line are statistically significant at the 95% confidence level.

Section 3d: Vertical Structure

To evaluate the ability of the CMIP5 models to represent the vertical structure of the GPLLJ, a vertical profile of the MAM meridional winds over the Great Plains, averaged over 25°-35°N, is shown for the 20CR (Fig. 7a), CFSR (Fig. 7b), and CMIP5 model mean (Fig. 7c). Both reanalyzes place the jet at similar longitudes (peaking at 97°-98°W) and levels (peaking at ~900 hPa), but the GPLLJ in the 20CR is approximately 0.5-1 m/s stronger at all levels, consistent with Fig. 2 for 850 hPa. The models simulate a MAM GPLLJ that is too weak by 1-2 m/s, which also agrees with previous results, but it is clear from Fig. 7 that the underestimation occurs throughout the vertical extent of the GPLLJ. The core of the GPLLJ is also located at a lower level in the troposphere (~925

hPa) than it is in the reanalyzes (~900 hPa). These results are consistent with the findings of Sheffield et al. (2013) that used fewer models. The models place the GPLLJ farther east than the reanalyzes by 1°-2° longitude, peaking it at 96°W. These issues could be due to horizontal and vertical resolutions in the models that are too coarse, making them unable to represent complex orographic features or PBL mechanisms such as those proposed by Blackadar (1957) and Holton (1967).

The JAS vertical profile, averaged over 30°-40°N, the latitudes used for the JAS GPLLJ index, is shown in Fig. 7d-f. The 20CR (Fig. 7d) has a similar GPLLJ position and intensity to the CFSR (Fig. 7e) at most levels, but the peak GPLLJ in the CFSR is approximately 1 m/s stronger. The model mean GPLLJ (Fig. 7f) is weaker than both reanalyzes by approximately 0.5-1 m/s, which is less than in MAM, consistent with previous results. As in the spring, the models place the peak wind too far east (by ~2°-3° longitude) and at a lower level in the troposphere (~925 hPa) than in the reanalyzes (~850-875 hPa).
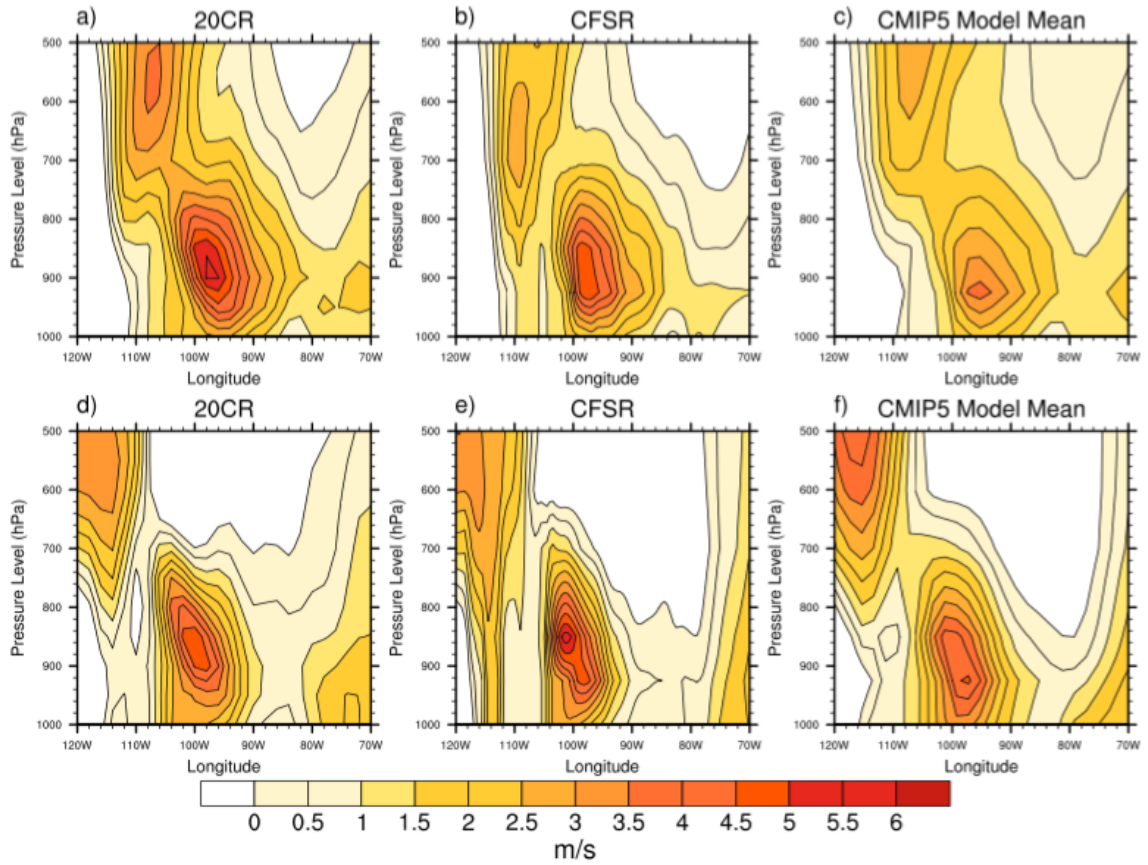
Figure 7: Lower-tropospheric mean vertical profile of MAM meridional wind averaged over 25°-35°N for the 20CR (a), CFSR (b), and CMIP5 model mean (c). The vertical profile of JAS meridional wind averaged over 30°-40°N for the 20CR (d), CFSR (e), and CMIP5 model mean (f).

Chapter 4: ENSO – GPLLJ Relationship

Section 4a: ENSO – GPLLJ Correlation

In addition to the climatology of the GPLLJ, it is very important to understand the ability of the CMIP5 models to simulate the mechanisms controlling the variability of the GPLLJ, and observations have shown that one of the most important mechanisms is ENSO (Schubert et al. 2004; Weaver et al. 2009; Muñoz and Enfield 2011; Krishnamurthy et al. 2015). To examine this mechanism in the models, the lagged cross-correlation between anomalies of the MAM GPLLJ index and previous December-January-February (DJF) ENSO in the 20CR, ERA20C, ERA-Interim, and CFSR are compared to the model mean correlation in Table 2. All four reanalyzes have a negative correlation which is significant at the 95% confidence level, agreeing with Muñoz and Enfield (2011) and Krishnamurthy et al. (2015). This suggests that a La Niña-like state in the tropical Pacific Ocean during winter is associated with a stronger GPLLJ in the following spring, while the opposite is true for El Niño. The model mean correlation is also significantly negative, but it is weaker than it is in the reanalyzes (Table 2).

To examine the spread in the DJF ENSO – MAM GPLLJ relationship among all the CMIP5 models, the standardized least-squares regression lines representing this relationship for each of the 131 ensemble members examined in this study are shown in Fig. 8a. Overall, 82 out of the 131 ensemble members (~63%) simulate a significant negative correlation, indicating that a majority are able to capture the observed relationship between ENSO and the GPLLJ in the spring. One ensemble member (from the MIROC-ESM model) simulates a significant positive correlation, while the rest are

insignificant. Similarly, 26 out of the 42 model means (~62%) demonstrate a significant negative correlation (Table A3).

Table 2 also shows the correlation between anomalies of the JAS GPLLJ index and previous DJF ENSO in the four reanalyzes and model mean. All reanalyzes demonstrate a shift to a positive correlation, meaning that a winter El Niño is associated with a stronger GPLLJ in the following summer, consistent with previous studies (Schubert et al. 2004; Weaver et al. 2009; Krishnamurthy et al. 2015). The correlation is significant in the 20CR and ERA20C but not in the ERA-Interim and CFSR, which can be attributed to the latter two reanalyzes covering fewer years. In contrast to the spring, the CMIP5 models are mostly unable to accurately simulate the ENSO – GPLLJ relationship in the summer, as the model mean correlation is very weakly negative (Table 2).

	20CR	ERA20C	ERA-Interim	CFSR	CMIP5 Model mean
MAM	**-0.36**	**-0.40**	**-0.36**	**-0.37**	**-0.24**
JAS	**0.28**	**0.29**	0.25	0.18	-0.08

Table 2: Linear cross-correlation between the DJF ENSO and following GPLLJ anomaly in MAM (top row) and JAS (bottom row). All correlations significant at the 95% confidence level are bolded.

Standardized regression lines representing the DJF ENSO – JAS GPLLJ relationship for each ensemble member are displayed in Fig. 8b. A shift toward a less negative correlation from the spring to the summer is apparent in the models, but 28 ensemble members (~21%) still simulate a significant negative correlation, and only two ensemble members (from BCC-CSM1.1-M and FGOALS-g2) simulate the significant

positive correlation that is seen in the reanalyzes (Fig. 8b). Furthermore, not a single model mean has a significant positive correlation (Table A4). These results demonstrate that the CMIP5 models do a very poor job representing the effects of ENSO on the GPLLJ in the summer, which agrees with the results that Krishnamurthy et al. (2015) found using the GFDL FLOR model. It is crucial that causes for this error are determined in order to improve our ability to understand and predict the summer GPLLJ in the future.
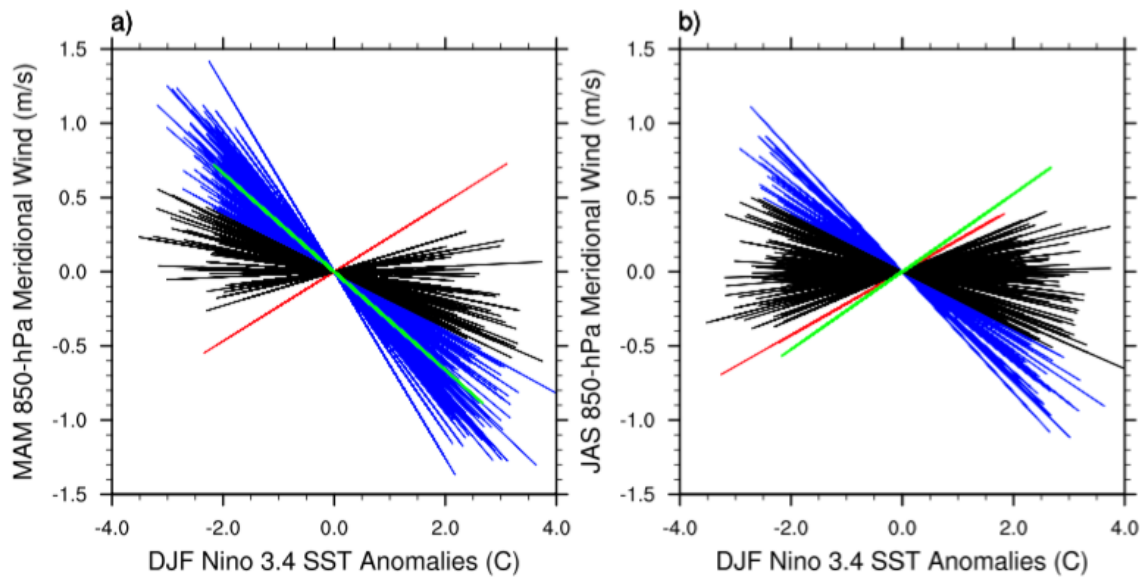
Figure 8: Standardized least-squares regression lines for each ensemble member representing the relationship between DJF ENSO and GPLLJ anomaly in the following MAM (a) and JAS (b). Blue (red) lines represent significant negative (positive) correlation at the 95% confidence level. The standardized regression line for the 20CR is in green.

Section 4b: Spatial Correlation

To examine the spatial extent and variability of the relationship between ENSO and the GPLLJ, the spatial correlation between DJF ENSO and the following MAM 850-hPa meridional wind anomalies is shown from the 20CR (Fig. 9a), ERA20C (Fig. 9b), ERA-Interim (Fig. 9c), CFSR (Fig. 9d), and CMIP5 model mean (Fig. 9e). In all four reanalyzes, there is a significant negative correlation over at least much of Texas, and in

27

the 20CR it exists over much of the Southern Plains, southeastern U.S., and GOM. The CMIP5 model mean also simulates a significant negative correlation over Texas, but it is weaker than in the reanalyzes (Fig. 9e). The area of strongest negative correlation in the reanalysis and in the models coincides with the placement of the core of the GPLLJ, and the placement of the GPLLJ in the models is very close to the reanalyzes, just slightly farther east (as seen in Fig. 7). The core of the GPLLJ in the model average is much weaker (peaking at ~3 m/s) than it is in the reanalyzes (peaking at 4.5-5.5 m/s), agreeing with the results from Section 3c.
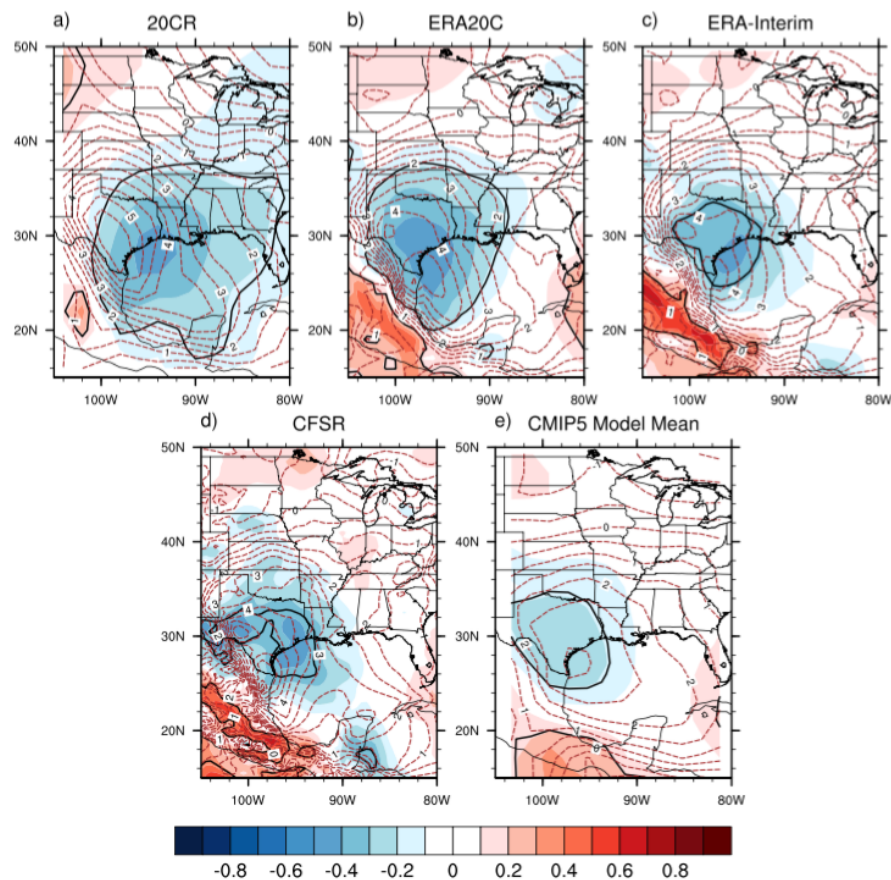
Figure 9: Cross-correlation between DJF ENSO and 850-hPa meridional wind anomalies in the following MAM (shading), and the mean MAM 850-hPa meridional wind over the period (brown dashed contours; contour interval 0.5 m/s) for the 20CR (a), ERA20C (b), ERA-Interim (c), CFSR (d), and CMIP5 model mean (e). All correlations within the bolded line are statistically significant at the 95% confidence level.

To determine whether simulation of the GPLLJ is affecting the models' ability to capture the accurate ENSO – GPLLJ relationship, the strength and position of the GPLLJ in the five models with the strongest negative DJF ENSO – MAM GPLLJ correlation, labeled the "best spring models" (Fig. 10a), is compared to the five models with the weakest negative DJF ENSO – MAM GPLLJ correlation, labeled the "worst spring models" (Fig. 10b). Overall, the differences in the GPLLJ between the two categories of models are not large. The worst models have a slightly weaker GPLLJ (peaking at ~2.5 m/s) than the best models (peaking at ~3 m/s), and while the worst models place the GPLLJ slightly farther east, this appears to be mainly due to the MIROC-ESM and MIROC-ESM-CHEM models, which place the core of the GPLLJ over the eastern GOM (not shown). Therefore, errors in simulating the intensity and location of the GPLLJ do not appear to be a major reason for the difficulty for some models to represent the observed ENSO – GPLLJ correlation in the spring.
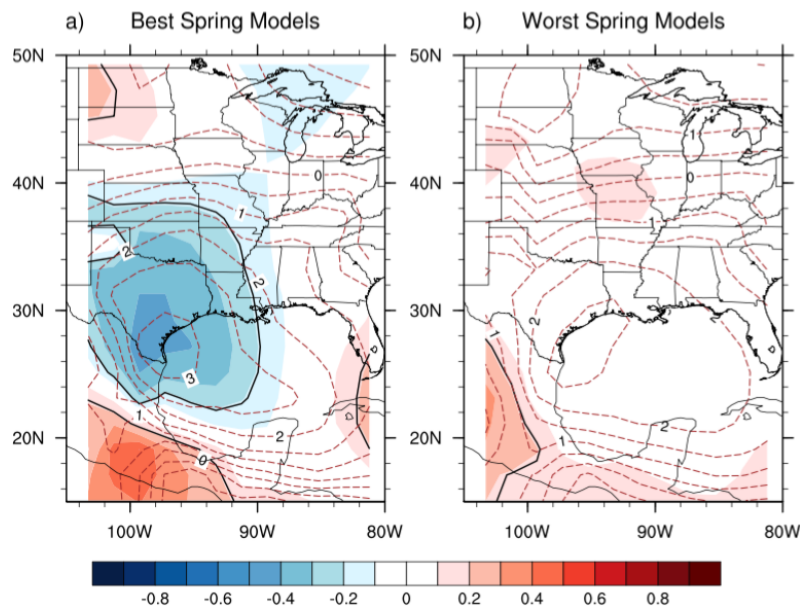
Figure 10: Same as Fig. 9, except for the mean of the five models with the strongest negative DJF ENSO - MAM GPLLJ correlation (a), and the mean of the five models with the weakest negative DJF ENSO - MAM GPLLJ correlation (b).

29

The analysis of the spatial correlation between DJF ENSO and the following JAS GPLLJ in the reanalyzes is shown in Fig. 11. A significant positive correlation exists over Texas northeastward to the upper Midwest in both the 20CR (Fig. 11a) and ERA20C (Fig. 11b) and over a much smaller region in the ERA-Interim (Fig. 11c). The CFSR has positive correlations over the Midwest, but none are significant (Fig. 11d). These correlations are shifted north from the spring, which corresponds with a northward movement of the GPLLJ. The GPLLJ also shifts west from the spring to the summer, which places the strongest positive correlations on the eastern side of the GPLLJ in the summer. This suggests that the GPLLJ is shifted to the east in summers following an El Niño event. However, consistent with previous results in this study, the CMIP5 model mean completely lacks this positive correlation anywhere over the Great Plains (Fig. 11e).
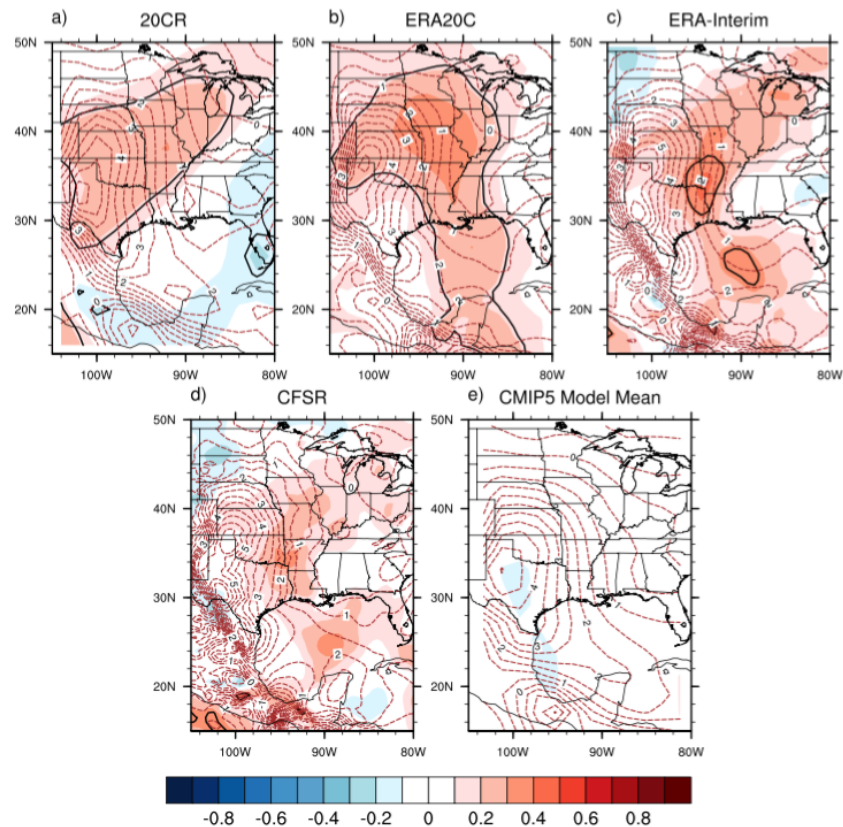
Figure 11: Same as Fig. 9, except for the JAS 850-hPa meridional wind.

Similar to the results found in the spring, the models' inability to simulate the observed ENSO – GPLLJ relationship in the summer does not appear to be due to poor model simulation of the location or intensity of the GPLLJ. The model mean places the core of the GPLLJ near the Texas panhandle, almost exactly where all four reanalyzes have it (Fig. 11e). The model mean GPLLJ core is only slightly weaker (peaking at ~5 m/s) than the reanalyzes (peaking at 5.5-6 m/s), and from Section 3c, the vast majority of models do not have errors in GPLLJ intensity that are statistically significant. Differences in the GPLLJ are examined between the five models with the most positive DJF ENSO – JAS GPLLJ correlation, labeled the "best summer models" (Fig. 12a), and the five models with the most negative DJF ENSO – JAS GPLLJ correlation, labeled the "worst summer models" (Fig. 12b). The worst models do have a weaker GPLLJ (peaking at ~4 m/s) than the best models (peaking at ~5.5 m/s), but the location of the GPLLJ is virtually the same in both groups of models. Furthermore, at least one model with a significant negative correlation (GFDL-CM2.1), simulates a GPLLJ that is nearly identical in strength and location to the reanalyzes (not shown). Therefore, it is not likely that a weak GPLLJ is a major factor in the failure of the models to capture the positive DJF ENSO – JAS GPLLJ correlation seen in the reanalyzes.
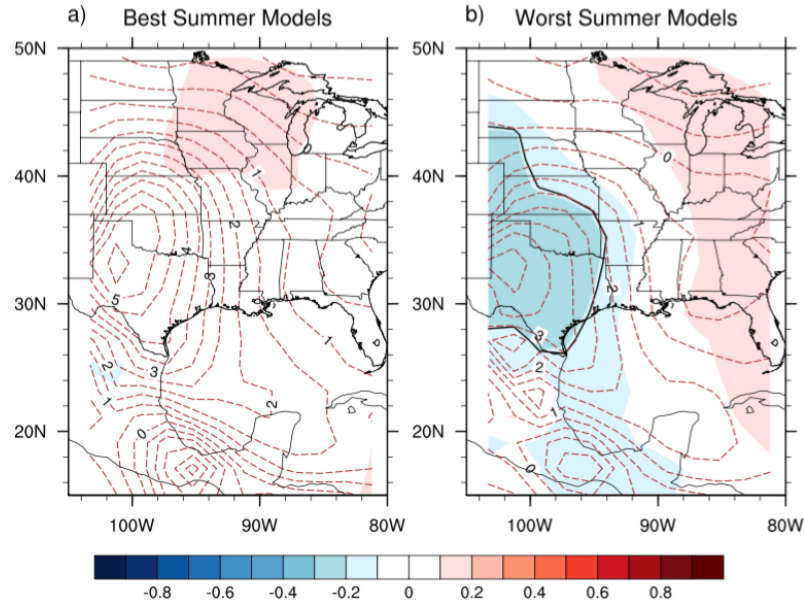
Figure 12: Same as Fig. 10, except for the JAS 850-hPa meridional wind, and for the models with the most positive DJF ENSO – JAS GPLLJ correlation (a), and the models with the most negative DJF ENSO – JAS GPLLJ correlation (b).

Section 4c: Effects on GPLLJ Characteristics

It is well-established that the GPLLJ is a daily phenomenon peaking in the nighttime hours, which causes nighttime precipitation events over the central U.S. (Stensrud 1996; Higgins et al. 1997; Weaver and Nigam 2008; Weaver et al. 2009). Therefore, it is also important to examine how ENSO affects the frequency and intensity of individual GPLLJ events in addition to the overall southerly flow in the Great Plains, in order to understand how it impacts the frequency and intensity of precipitation events in the Great Plains. The time of day examined is 06Z, which is when the GPLLJ is strongest in the ERA-Interim and CMIP5 models (Fig. 3), agreeing with previous studies (Higgins et al. 1997; Jiang et al. 2007; Pu and Dickinson 2014). As shown in Table 3 and expected from prior results presented here, and in other studies, the average 850-hPa meridional wind in the ERA-Interim over all days in MAM following DJF La Niñas is

32

significantly stronger (at the 95% confidence level) than it is following DJF El Niños, with the reverse relationship holding for the JAS 850-hPa meridional wind.

However, when only including days that have a GPLLJ "event", defined here as 850-hPa meridional wind that is at least one standard deviation above the mean, there is no statistically significant difference in the strength of the MAM GPLLJ between El Niño and La Niña years in the ERA-Interim (Table 3). Instead, the influence of ENSO is on the frequency of MAM GPLLJ events, as nearly five more events occur per year on average following DJF La Niña events compared to El Niño events (~37% increase), a difference that is statistically significant. This may be due to La Niña events resulting in more frequent (but not necessarily more intense) high SLP anomalies over the IAS, which Krishnamurthy et al. (2015) found to play a critical role in the mechanism that drives the relationship between ENSO and the MAM GPLLJ. In JAS, GPLLJ events following DJF El Niños are significantly more frequent (by ~62%) and significantly more intense than GPLLJ events following DJF La Niñas, so both frequency and intensity are affected (Table 3). A possible reason for this is that El Niño events result in more frequent and more intense high SLP anomalies over the tropical Atlantic in the summer, which causes more frequent and more intense GPLLJ events, following the mechanistic hypothesis explaining the ENSO – GPLLJ teleconnection in the summer proposed by Krishnamurthy et al. (2015).

	MAM		JAS	
	El Niño	La Niña	El Niño	La Niña
Average Meridional Wind (m/s)	**3.76**	**4.92**	**5.80**	**5.12**
Average GPLLJ Event (m/s)	12.92	12.98	**11.80**	**11.21**
Number of GPLLJ Events Per Year	**12.5**	**17.2**	**17.0**	**10.5**

Table 3: Effects of DJF ENSO on the mean daily 850-hPa meridional wind, mean GPLLJ event, and frequency of GPLLJ events in MAM and JAS over the GPLLJ index regions in the ERA-Interim. See text for the definition of a GPLLJ event. Values are bolded if the difference between them is statistically significant at the 95% level.

To analyze the spatial distribution of ENSO's influence on GPLLJ intensity, the difference in MAM meridional wind during GPLLJ events between years following DJF El Niño and La Niña events in the ERA-Interim is shown in Fig. 13a. To the northeast of the strongest MAM GPLLJ, a large change is evident as the meridional wind is at least 1.8-2 m/s stronger following El Niños compared to La Niñas, while just to the west of the peak of the GPLLJ over western Texas, the meridional wind is 1-2 m/s weaker (Fig. 13a). However, over most of the MAM GPLLJ index region used in this study, there is little change in meridional wind strength between El Niño and La Niña years during GPLLJ events, agreeing with the results from Table 3. This indicates that ENSO may be having the expected effect on MAM GPLLJ event intensity (stronger GPLLJ following La Niñas than El Niños) near where the GPLLJ is strongest, but this influence does not extend into the rest of the GPLLJ. The difference in average annual frequency of MAM GPLLJ events at each grid point between years following DJF El Niño and La Niña events is shown in Fig. 13b. Two to six more GPLLJ events occur per year following La Niña

events than El Niño events over much of Oklahoma and Texas, where the GPLLJ is

strongest in MAM. This demonstrates that the effect of ENSO on MAM GPLLJ

frequency exists over a much larger area than the effect on MAM GPLLJ intensity.
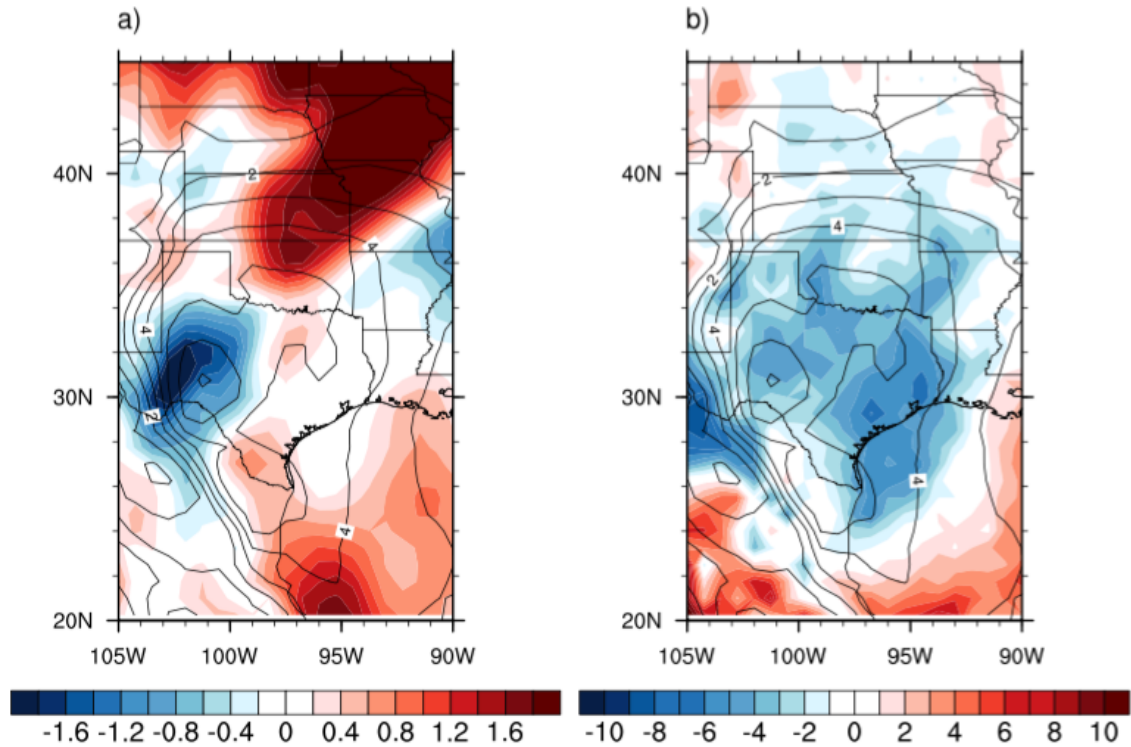
Figure 13: The difference in MAM meridional wind (m/s) during GPLLJ events (a) and the difference in average annual frequency of MAM GPLLJ events at each grid point (b) between years following DJF El Niño and La Niña events in the ERA-Interim. See text for the definition of a GPLLJ event. The mean MAM meridional wind is plotted as black contours (contour interval 1 m/s).

The analysis of the effects of ENSO on GPLLJ characteristics is shown in Fig. 14

for JAS. In contrast to MAM, the JAS meridional wind in the ERA-Interim during GPLLJ

events is clearly affected by ENSO over a large region (Fig. 14a). This region

encompasses much of eastern Texas, the Texas panhandle, Oklahoma, southeastern

Kansas, and central Missouri, where the meridional wind is stronger following DJF El

Niño events than DJF La Niña events (by 0.6-1.4 m/s). The average frequency of JAS

GPLLJ events is also substantially higher following DJF El Niños compared to DJF La Niñas (by 3-8 events per year) over this same area (Fig. 14b). Consistent with Table 3, these results show that ENSO has a widespread influence on both the frequency and intensity of GPLLJ events over the central U.S. in JAS.
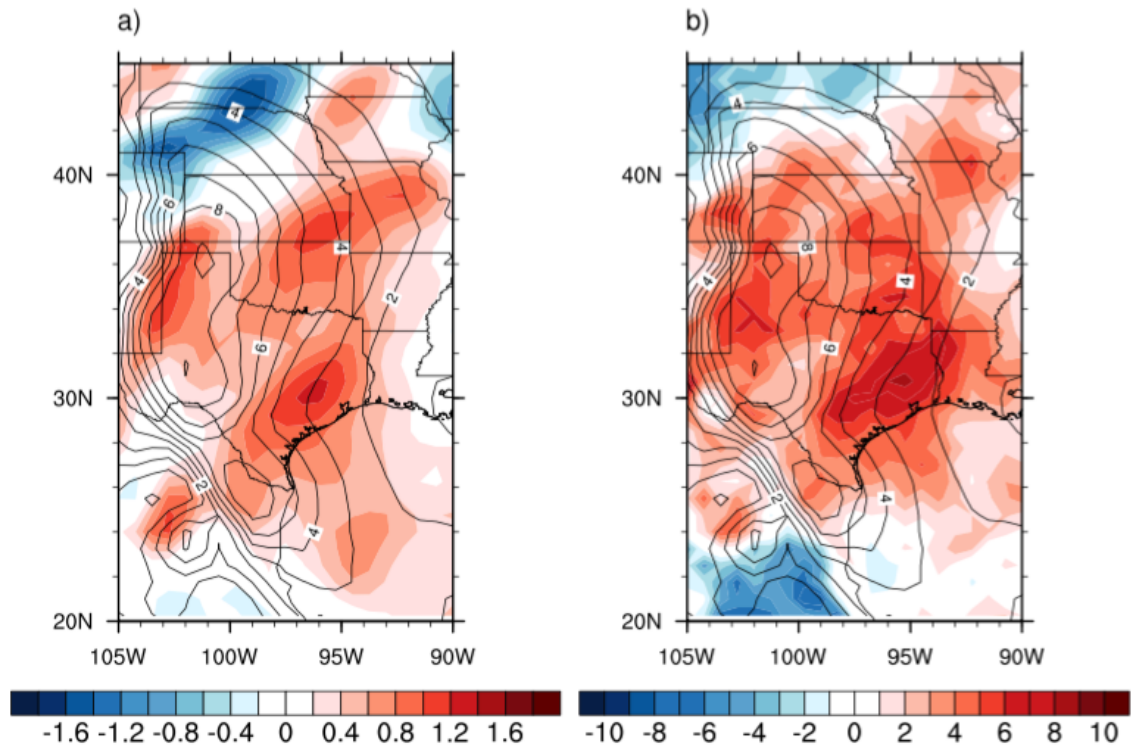
Figure 14: Same as Fig. 13, but for the JAS meridional wind.

The ability of the CMIP5 models to capture the observed influence of ENSO on the frequency and intensity of GPLLJ events is examined in order to improve predictions of these GPLLJ characteristics. For example, the GPLLJ has been shown to play a significant role in severe weather outbreaks over the Great Plains (Lee et al. 2013), so it is important to accurately predict whether a certain ENSO event will result in severe weather events that are more frequent, more intense, or both. One ensemble member each from three models (CNRM-CM5, FGOALS-g2, and MIROC-ESM) are used for this

analysis. As shown in Table 4, only the CNRM-CM5 model simulates a significant (at the 95% confidence level) influence on the average MAM 850-hPa meridional wind, with the flow significantly stronger following DJF La Niña events than DJF El Niño events. Furthermore, there is little difference in the mean MAM GPLLJ event strength in this model between El Niño and La Niña years, but the frequency of GPLLJ events increases significantly following La Niñas compared to El Niños (by ~79%), consistent with the ERA-Interim (Table 3). In the FGOALS-g2 model, the frequency and intensity of MAM GPLLJ events exhibit no significant change following El Niño and La Niña events, while the MIROC-ESM model does simulate a significant difference in the intensity of the GPLLJ. However, there is no significant change in the frequency of GPLLJ events, which indicates that this model is still unable to capture the accurate effects of ENSO on the characteristics of the GPLLJ. From Table 4 it is also clear that none of the models simulate the influence of ENSO on the mean JAS GPLLJ seen in the ERA-Interim, agreeing with the previous results in this study. The differences in the average meridional wind, average GPLLJ event, and frequency of GPLLJ events are insignificant in all three models.

	MAM						JAS					
	CNRM-CM5		FGOALS-g2		MIROC-ESM		CNRM-CM5		FGOALS-g2		MIROC-ESM	
	El Niño	La Niña	El Niño	La Niña	El Niño	La Niña	El Niño	La Niña	El Niño	La Niña	El Niño	La Niña
Average Meridional Wind (m/s)	**2.81**	**4.52**	2.11	2.41	3.04	3.04	5.90	5.95	4.52	4.50	5.92	5.68
Average GPLLJ Event (m/s)	12.44	12.18	9.62	9.75	**10.79**	**11.26**	11.59	11.69	10.17	10.07	12.84	13.15
Number of GPLLJ Events Per Year	**9.9**	**17.7**	14.8	14.8	15.7	16.1	14.0	13.3	15.8	15.8	16.9	15.5

Table 4: Same as Table 3, but for three CMIP5 models.

Chapter 5: Factors Affecting ENSO – GPLLJ Relationship in CMIP5

Section 5a: Effects of ENSO Intensity

In order to better develop our understanding of the relationship between the GPLLJ and ENSO, we must determine whether this relationship is linear, or if it depends on the strength of the ENSO event. Fig. 15a shows the difference from the mean MAM GPLLJ following weak, moderate, and strong DJF ENSO events in the 20CR. Weak, moderate, and strong El Niño (La Niña) events are defined as SST anomalies ≥ 1 and $<$ 1.5, ≥ 1.5 and < 2, and ≥ 2 standard deviations above (below) the mean, respectively. Based on results from this study and from past studies (Muñoz and Enfield 2011; Krishnamurthy et al. 2015), a weaker MAM GPLLJ would be expected following El Niño events and a stronger MAM GPLLJ would be expected following La Niña events. From Fig. 15a, it is apparent that this relationship does not hold for weak ENSO events in the 20CR, as the MAM GPLLJ is weaker following weak El Niños and weak La Niñas. ENSO events need to have at least moderate intensity to have the expected influence on the GPLLJ, with the GPLLJ as much as 1.5 m/s stronger than the mean following moderate El Niños and as much as 0.75 m/s weaker following moderate La Niñas. The GPLLJ is as much as 2.5 m/s weaker and stronger than the mean during strong El Niño and strong La Niña years, respectively, so this effect is amplified even further following strong ENSO events. Furthermore, as was found in Fig. 9a, the maximum influence of ENSO in the 20CR appears to be on the eastern side of the MAM GPLLJ, over eastern Texas and Louisiana (Fig. 15a).

As shown in Fig. 15b, the CMIP5 model mean simulates a weaker-than-average MAM GPLLJ following all El Niño events and a stronger-than-average MAM GPLLJ

following all La Niña events, agreeing with the 20CR. In contrast to the reanalysis, however, this relationship is true for weak ENSO events, and while the GPLLJ is weakest following strong El Niño events, the GPLLJ is strongest following moderate La Niña events. This indicates that the influence of La Niña events on the GPLLJ in the models does not necessarily increase with increasing La Niña event intensity, as it does in the 20CR. Furthermore, the differences in GPLLJ intensity are not as large for moderate and strong ENSO events as they are in the 20CR. This is likely at least partially due to averaging over many models. The spatial patterns are also different from the 20CR, as the maximum influence of ENSO on the strength of the GPLLJ occurs over much of Texas, at the core of the GPLLJ (consistent with Fig. 9e), which is to the west of where the strongest influence occurs in the 20CR. Lastly, it is interesting to note that the "worst spring models" do an especially poor job simulating the observed influence of strong La Niñas on the GPLLJ (Fig. B3). The GPLLJ in these models is as much as 1.2 m/s weaker following strong La Niñas, while the 20CR shows that it should be up to 2.5 m/s stronger (Fig. 15a).
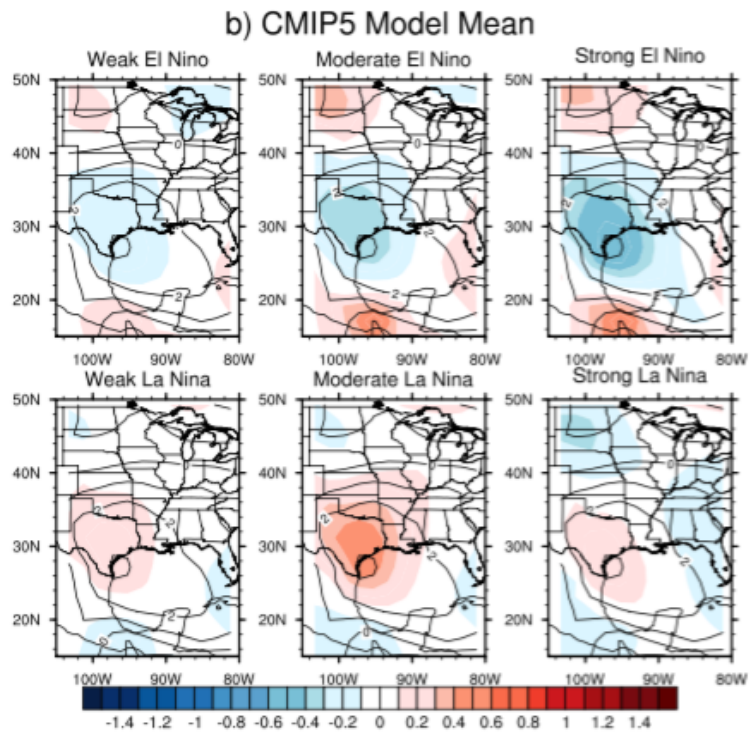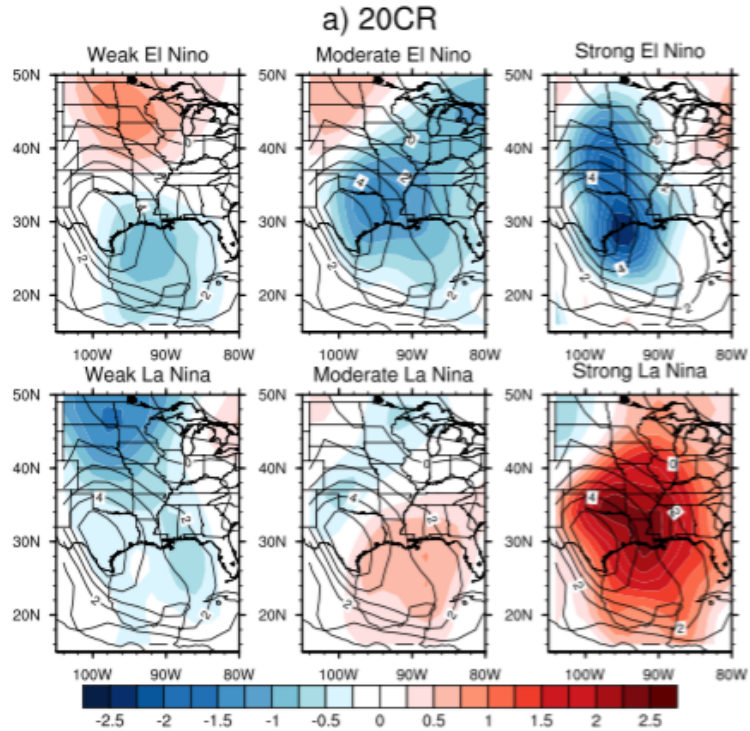
Figure 15: Difference from mean MAM 850-hPa meridional winds following weak, moderate, and strong DJF ENSO events (shading) and mean MAM 850-hPa meridional winds (black contours; contour interval 1 m/s) in the 20CR (a) and CMIP5 model mean (b).

The analysis is conducted for the JAS GPLLJ and is shown in Fig. 16. As expected, the JAS GPLLJ is stronger following DJF El Niño events and weaker following DJF La Niña events in the 20CR (Fig. 16a). The largest changes in the strength of the JAS GPLLJ shift northwestward from MAM, and they are located close to the peak of the GPLLJ, except following strong El Niños when the GPLLJ is shifted to the north. However, this relationship only exists for ENSO events of moderate to strong intensity, especially for strong ENSO events as the JAS GPLLJ is ~4 m/s more intense following strong El Niños than it is following strong La Niñas. Consistent with the results in MAM, the JAS GPLLJ exhibits very little change in strength following weak ENSO events (Fig. 16a). This analysis demonstrates that the influence of ENSO on the GPLLJ is not linear but is heavily dependent on the strength of the ENSO event, which can be used to more accurately predict the strength of the GPLLJ in the future.

Unlike the reanalysis, the CMIP5 model mean simulates very little influence of DJF ENSO on the JAS GPLLJ, and the small relationship that does exist is the opposite of the 20CR (Fig. 16b). This also agrees with the previous findings from this study. The JAS GPLLJ in the CMIP5 model mean is 0.1-0.3 m/s weaker following El Niño events and 0.1-0.3 m/s stronger following La Niña events. Strong ENSO events still have the largest influence on GPLLJ intensity, but the influence is only slightly greater than it is for weak and moderate ENSO events. The models simulate these differences over the core of the JAS GPLLJ in Texas and Oklahoma, near the location of the differences in the 20CR. As was found in the spring, the "worst summer models" particularly struggle to represent the accurate effects of strong La Niñas on the JAS GPLLJ (Fig. B4). The

GPLLJ in these models is as much as 1.3 m/s stronger following strong La Niñas, while

the 20CR shows that it should be up to 2.25 m/s weaker (Fig. 15a).
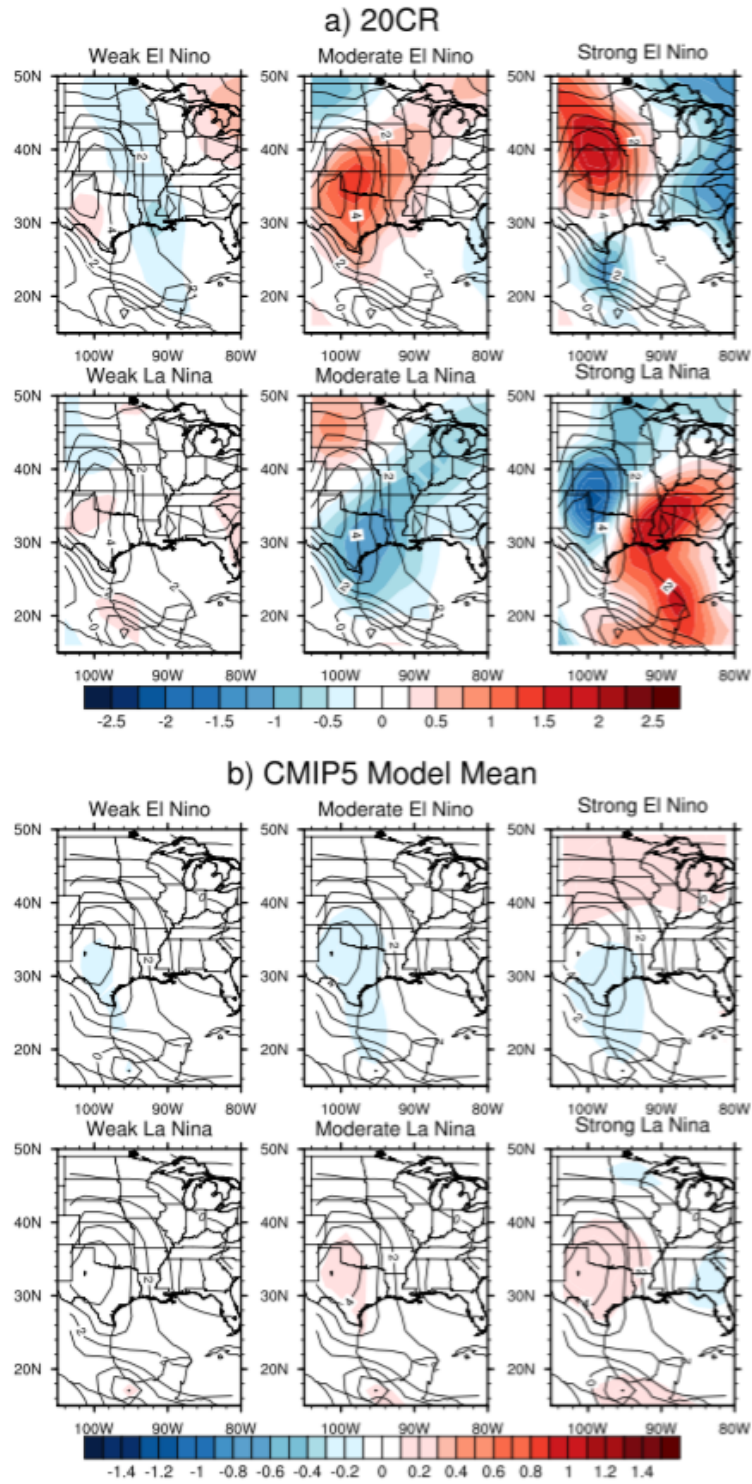
Figure 16: Same as Fig. 15, but for JAS 850-hPa meridional winds.

Section 5b: ENSO SST Patterns

As this study has shown, some CMIP5 models struggle to represent the observed DJF ENSO – MAM GPLLJ relationship, and none of them are able to simulate the observed DJF ENSO – JAS GPLLJ relationship. This inability is not due to their representation of the GPLLJ (see Chapter 4, Section b). To determine whether this could be due to a poor simulation of the strength or structure of ENSO, the average DJF SST anomalies during El Niño events in the HadISST1 (Fig. 17a) and ERSST (Fig. 17b) are compared to the CMIP5 model mean (Fig. 17c). El Niño events have the same strength in both the HadISST1 and ERSST, and the meridional width of SST anomalies associated with El Niños is comparable in both sets of observations. However, the peak strength of SSTs associated with El Niños extend farther east in the HadISST1 than they do in the ERSST. It is apparent that the CMIP5 model mean is mostly able to capture the strength of El Niño events, though SST anomalies in the north Pacific and the Atlantic are minimal compared to observations. The spatial extent of SSTs associated with El Niño events in the CMIP5 model mean is similar to the HadISST1, but it is farther east than the ERSST (peaking near 120°W in the models compared to near 150°W in the ERSST). Also included in Fig. 17 are the SST anomalies in the "best spring models" (Fig. 17d) and "worst spring models" (Fig. 17e). The worst models also have El Niño events that are too weak (by ~0.8°C) compared to observations, while El Niño events in the best models are approximately 0.4°C stronger than observations.

During La Niña (Fig. 18), the HadISST1 (Fig. 18a) has SST maxima that are ~0.2°C weaker than the ERSST (Fig. 18b), and similar to El Niños, the peak SST anomalies are slightly farther east in the HadISST1. The CMIP5 model mean (Fig. 18c)

simulates the SST maxima too far east (near 120°W) compared to observations (near 130°-150°W) (Figs. 18a,b). Furthermore, in the model mean the meridional width of SSTs associated with La Niñas is too narrow and SST anomalies in the rest of the Pacific and the Atlantic are too weak. The worst models (Fig. 18e) simulate La Niña events substantially weaker (by ~1°C) than the best models (Fig. 18d), but only ~0.2 m/s weaker than the ERSST and nearly identical to the HadISST1. Since the SST pattern associated with ENSO is simulated weaker in the worst models, its effects on the overall atmospheric circulation, and thus on the mechanisms that drive the GPLLJ, are likely lessened as well. This indicates that some of the models' inability to capture the negative DJF ENSO – MAM GPLLJ correlation seen in observations may be due to a simulation of ENSO SST anomalies that are too weak. ENSO SST patterns were also examined in the "best summer models" and "worst summer models", but in contrast to the spring, the worst models in the summer do not simulate a weaker ENSO SST pattern than the best models (not shown). Therefore, this does not appear to be a driving factor behind the models' inability to simulate the positive correlation between ENSO and the JAS GPLLJ.
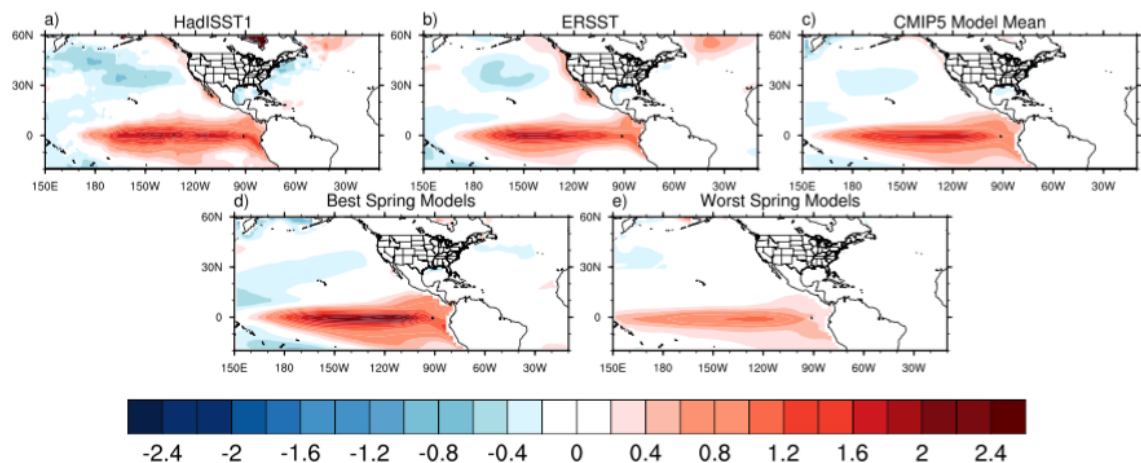
Figure 17: Mean DJF SST anomalies (°C) during DJF El Niño for the HadISST1 (a), ERSST (b), CMIP5 model mean (c), "best spring models" (d), and "worst spring models" (e).
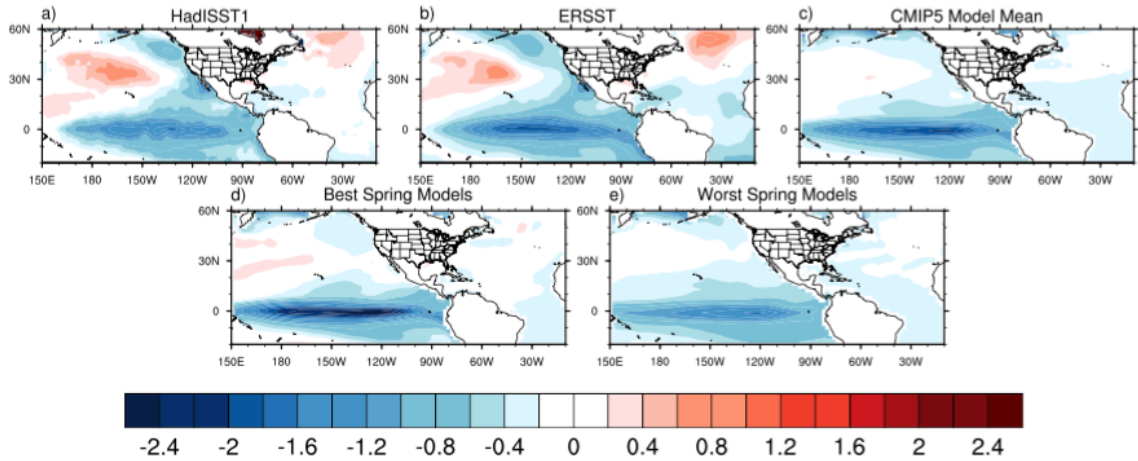
Figure 18: Same as Fig. 17, but for La Niña.

Section 5c: Atmospheric Response to ENSO

If CMIP5 models are unable to represent the atmospheric response to ENSO, they will not be capable of capturing the observed effects of ENSO on the GPLLJ. According to Hurwitz et al. (2014), CMIP5 models are able to simulate the observed upper tropospheric responses to ENSO in boreal autumn and winter. This includes increased upper tropospheric geopotential heights in the eastern tropical Pacific but decreased heights in the western tropical Pacific from El Niño events. The North Pacific and South Pacific lows in the models also deepen during El Niño events and weaken during La Niña events (Hurwitz et al. 2014). The teleconnections that drive the relationship between an ENSO-PDO mode and North American winter precipitation are reproduced well in the CMIP5 models (Polade et al. 2013).

The influence of ENSO on MAM 850-hPa geopotential heights is examined in Fig. 19. Using the 20CR (Fig. 19a), ERA20C (Fig. 19b), and ERA-Interim (Fig. 19c) reanalysis, DJF ENSO is shown to be negatively correlated with MAM 850-hPa geopotential heights over the eastern Pacific and western Atlantic and positively

correlated in the western Pacific, agreeing with previous studies (Shinker and Bartlein 2009). The CMIP5 model mean (Fig. 19d) and "best spring models" (Fig. 19e) are successful at representing this relationship, while the "worst spring models" simulate the observed pattern but it is too weak (Fig. 19f). This gives further evidence to the hypothesis that these models are struggling to represent the correct ENSO - GPLLJ relationship in the spring because they are simulating ENSO that is too weak, and thus it is not having enough influence on geopotential heights which are one of the most important drivers of GPLLJ variability.
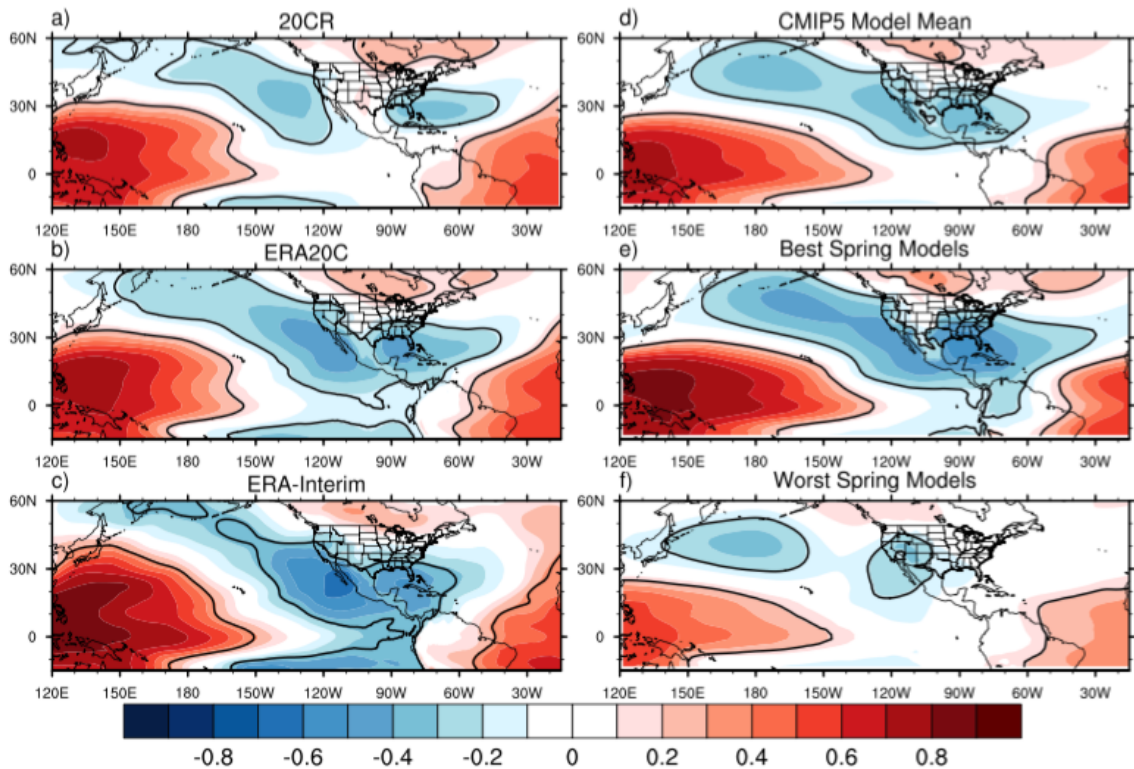
Figure 19: Lagged correlation between MAM 850-hPa geopotential height anomalies and the previous DJF ENSO in the 20CR (a), ERA20C (b), ERA-Interim (c), CMIP5 model mean (d), "best spring models" (e), and "worst spring models" (f). All correlations within the bolded line are statistically significant at the 95% confidence level using a two-tailed probability test.

The correlation between DJF ENSO and the following JAS 850-hPa geopotential heights is also examined in the 20CR (Fig. 20a), ERA20C (Fig. 20b), and ERA-Interim (Fig. 20c). A negative correlation is observed in the northern and western U.S., while a positive correlation is observed in the southeastern U.S. This height gradient is an essential mechanism of the GPLLJ (Harding and Snyder 2015). However, the CMIP5 model mean is mostly unable to simulate this gradient associated with ENSO, as it exhibits a slight (but insignificant) positive correlation across the eastern and western U.S. (Fig. 20d). The "worst summer models" do a particularly poor job because they simulate a significant positive correlation over the western U.S. (Fig. 20f). The correlation between DJF ENSO and JAS 850-hPa geopotential heights is shown in Fig. 20e for the model that simulates the most positive (closest to observed) DJF ENSO – JAS GPLLJ correlation (CMCC-CMS), though it is still not significant. It is apparent that this model is more successful in comparison to the model mean, as it simulates the height gradient across the U.S. (positive correlation in the eastern U.S. and negative correlation in the north-central U.S.) that is seen in the reanalyzes. Therefore, it appears that the models' inability to simulate the positive DJF ENSO – JAS GPLLJ relationship seen in observations can be at least partially attributed to an inaccurate representation of the effects of ENSO on geopotential heights in the following summer across the U.S.
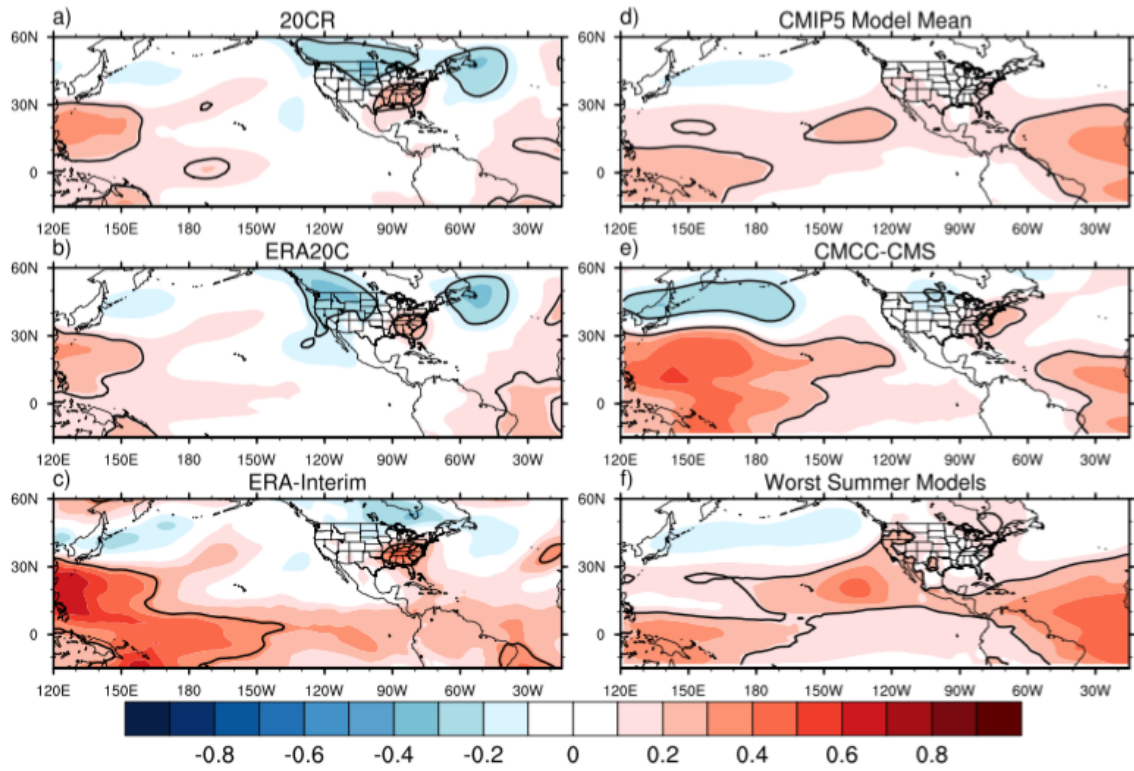
Figure 20: Same as Fig. 19, but for JAS 850-hPa geopotential height anomalies.

Chapter 6: Discussion and Conclusions

Section 6a: Summary

The goal of this study was to investigate the ability of the CMIP5 models to represent some of the most important features and mechanisms of the GPLLJ in their historical simulations, as well as reasons for successful and unsuccessful simulations. Based on the results from this study, a nocturnal GPLLJ exists in the CMIP5 models, and some overall features of the GPLLJ in the models are comparable to the reanalyzes. However, several important details differ. One of the most striking errors is the models' underestimation of the strength of the GPLLJ in the spring. The MAM model mean GPLLJ is significantly weaker than the 20CR, and a majority of models (25 out of 42) simulate a MAM GPLLJ that is significantly weaker. This is a critical finding because if the GPLLJ in the models is too weak, it is likely that the models will be unable to fully capture the extent of its influence on precipitation and severe weather over the Great Plains. In JAS, the model mean GPLLJ is not significantly different from the 20CR, and only a small minority of models have a GPLLJ that is significantly different (six weaker and three stronger). It is shown that a contributing factor to some of the models' inability to reproduce the observed GPLLJ intensity in MAM and JAS could be simulating a pressure gradient across the central U.S. that is too weak.

In addition to strength, the location and timing of the GPLLJ in the CMIP5 models differ from the reanalyzes in a number of ways. The core of the GPLLJ is located at a lower level in the models (~925 hPa) than in the reanalyzes (~900 hPa in the spring and ~850-875 hPa in the summer). These results agree with the findings from Sheffield et al. (2013). The GPLLJ in the models is also located farther east than it is in the reanalyzes.

50

While the seasonal cycle of the GPLLJ in the models is similar to the reanalyzes, the models extend its peak too late in the summer, again consistent with Sheffield et al. (2013). Out of the three CMIP5 models whose daily GPLLJ data was examined in this study (CNRM-CM5, FGOALS-g2, and MIROC-ESM), all three reproduce the observed peak of the GPLLJ at 06Z in the spring and summer seen in the ERA-Interim and in previous studies (Higgins et al. 1997; Jiang et al. 2007; Pu and Dickinson 2014), but in two of the models, the daily minimum of the MAM GPLLJ occurs at 12Z instead of the observed minimum at 00Z. These errors in location and timing of the GPLLJ could be having a considerable negative impact on the models' ability to accurately predict heavy rainfall and severe weather events in the central U.S. Therefore, it is crucial that causes for these errors are determined, which should be a subject of future research.

Analysis of reanalyzes/observations demonstrate that ENSO has a significant impact on the strength of the GPLLJ, with a significant negative correlation in the spring and a significant positive correlation in the summer, consistent with prior studies (Schubert et al. 2004; Weaver et al. 2009; Muñoz and Enfield 2011; Krishnamurthy et al. 2015). The majority of CMIP5 ensemble members (82 out of 131) capture the significant negative DJF ENSO – MAM GPLLJ correlation seen in the reanalyzes, and the models and reanalyzes generally agree on the placement of this correlation over the core of the GPLLJ. However, in contrast to the reanalyzes, the model mean DJF ENSO – JAS GPLLJ correlation is weakly negative, and only two out of 131 ensemble members capture the observed significant positive correlation. This means that some models are unable to simulate the observed influence of ENSO on the GPLLJ in the spring, and the vast majority of models are unable to represent the observed influence of ENSO on the GPLLJ

in the summer, which is likely inhibiting the accuracy of their near- and long-term predictions and projections of the GPLLJ.

It is shown that the inability of the CMIP5 models to simulate the influence of ENSO on the GPLLJ is not due to errors in simulating the intensity and location of the GPLLJ. Instead, the failure of some models to represent the observed negative DJF ENSO – MAM GPLLJ correlation can be attributed to simulating ENSO SST patterns that are too weak, which makes the atmospheric response to ENSO too weak. This response includes the high geopotential height anomalies over the GOM and Caribbean Sea in MAM that result from La Niña events, which have been shown to play a crucial role in the mechanism that drives the correlation between ENSO and the GPLLJ in the spring (Krishnamurthy et al. 2015).

In the summer, on the other hand, the failure of nearly all of the CMIP5 models to reproduce the observed influence of ENSO on the GPLLJ is not due to simulating ENSO SST patterns that are too weak. Instead, it can be attributed to a very poor representation of the impact of DJF ENSO on 850-hPa geopotential heights across the U.S. in the following JAS. According to the reanalyzes, DJF El Niño events should result in negative geopotential height anomalies across the north-central and western U.S. and positive geopotential height anomalies across the southeastern U.S. in the following JAS. As was shown by Harding and Snyder (2015), this height gradient is an important mechanism of the GPLLJ. However, the model mean is mostly unable to simulate this height pattern, while the model that is most successful at simulating the observed positive DJF ENSO – JAS GPLLJ correlation (CMCC-CMS) does simulate the height gradient across the U.S. that is seen in the reanalyzes (though it is still weaker). These results

indicate that our predictions and projections of the variability of the GPLLJ (and thus of precipitation and severe weather across the Great Plains) could be greatly improved in future generations of climate models if some models are able to simulate stronger SST patterns associated with ENSO, and if all models are able to more accurately represent the summertime atmospheric response to ENSO across the U.S.

This study further examined the observed relationship between ENSO and the GPLLJ by analyzing whether it depends on the strength of the ENSO event. In the 20CR, it is found that weak ENSO events have minimal to no impact on the strength of the GPLLJ in both the spring and summer. Moderate and strong ENSO events have the expected influence, especially strong ENSO events as the MAM (JAS) GPLLJ is ~4-5 m/s stronger (weaker) following strong DJF La Niñas than strong DJF El Niños. These results show that the intensity of the ENSO event does matter for the ENSO - GPLLJ relationship, which should be taken into consideration when using the state of ENSO to make predictions of the GPLLJ.

In addition, the influence of ENSO on the frequency and intensity of individual GPLLJ events was investigated. It is found in the ERA-Interim that the statistically significant effect of ENSO is on the frequency, not intensity, of GPLLJ events in the spring, while both frequency and intensity are significantly affected in the summer. These results have very important implications for the use of the ENSO - GPLLJ relationship to make weather predictions over the Great Plains, because these individual daily GPLLJ events are what drive heavy precipitation events. Since ENSO affects the frequency, not intensity, of MAM GPLLJ events, it is likely that DJF La Niñas (El Niños) will result in more (less) frequent heavy rainfall and severe weather events in the spring across the

Central U.S., but they will not necessarily be more intense. In the summer, however, both the frequency and intensity of heavy rainfall and severe weather events will likely increase (decrease) following DJF El Niños (La Niñas). The effects of ENSO on GPLLJ characteristics was also examined in three CMIP5 models (CNRM-CM5, FGOALS-g2, and MIROC-ESM), and it was discovered that only the CNRM-CM5 model is able to capture the accurate influence (significantly more frequent, but not more intense, GPLLJ events following La Niñas) in the spring. None of the models simulate the observed impact of ENSO on GPLLJ characteristics in the summer, consistent with the previous results.

While past studies, including Sheffield et al. (2013), have investigated the ability of small subsets of CMIP5 models to simulate some of the observed features of the GPLLJ, this study is unique for several reasons. No prior research had examined this ability in the entire suite of CMIP5 models, nor had it analyzed the diurnal cycle of the GPLLJ in any CMIP5 simulations. Furthermore, this is the first time a study has examined the ability of CMIP5 models to represent the observed relationship between ENSO and the GPLLJ, as well as factors affecting their ability to do so. Investigating the influence of ENSO on the frequency and intensity of daily GPLLJ events in reanalyzes and CMIP5 models had also never been conducted before this study. These new findings will play an important role in improving predictions and projections of Great Plains weather and climate.

Section 6b: Limitations and Future Work

This study has a number of limitations and assumptions that should be considered, and future research should be done to explore the significance of these limitations and how they can be reduced. One major assumption is the accuracy of the four reanalyzes used in this study (20CR, ERA20C, ERA-Interim, and CFSR) in their representation of the GPLLJ. As shown by Berg et al. (2015), the ERA-Interim and CFSR (in addition to the NCEP2, JRA-25, MERRA, and NARR reanalyzes) suffer from several biases in the GPLLJ compared to observations. They overestimate the wind speed between the core of the GPLLJ (at ~900 hPa) and the 800 hPa pressure level, and they place the core of the GPLLJ at a higher altitude than the observations. These biases could mean that two of the errors in CMIP5 model simulation of the GPLLJ that were found in this study, placing the GPLLJ too low in the atmosphere and simulating a GPLLJ that is too weak, may have been overestimated. In fact, the model mean GPLLJ using the height of maximum wind in the models (925 hPa) instead of in the reanalyzes (850 hPa) is stronger than it was at 850 hPa, though it is still weaker than the reanalysis mean for all months of the year outside of JAS (not shown). In addition, it has been found that reanalyzes (including the ERA-Interim and CFSR) underestimate the frequency of GPLLJ events, particularly strong GPLLJ events (Berg et al. 2015). This problem is especially prevalent among the reanalyzes with coarser resolutions such as the ERA-Interim, which could limit the reliability of the results from Section 4c (and potentially other parts of this study as well). The 20CR and ERA20C have even lower resolutions than the ERA-Interim, which could also be limiting their ability to accurately depict various features of the GPLLJ. According to Berg et al. (2015), the relatively high-resolution CFSR has much better agreement with

55

observations on the frequency of strong GPLLJ events, which indicates that high-resolution reanalyzes such as the CFSR might be more reliable in their depiction of the GPLLJ. Therefore, the accuracy of observed GPLLJ features and mechanisms may be improved in future studies by increasing the resolution of reanalyzes such as the ERA-Interim, or by only using high-resolution reanalyzes for depicting the observed GPLLJ. However, other factors besides resolution could be important as well, and additional research is needed to identify these factors and their causes, in order to develop improved reanalysis products. Increasing the coverage and availability of wind observations could also be beneficial for future studies of the GPLLJ.

Another limitation of this study is the relatively small number of ENSO events in the observations, particularly strong events as there are only two strong El Niños and one strong La Niña. In contrast, there are 392 strong El Niño events and 222 strong La Niña events among all the CMIP5 ensemble members. These very large differences in sample sizes between the models and the observations could be an important factor in the disparity between the models and 20CR regarding the influence of strong ENSO events on the GPLLJ. The magnitude of this influence is much smaller in the model mean, but this could be largely due to averaging over so many events in the models compared to the 20CR. Therefore, confidence in this comparison is low, and a larger number of ENSO events in the observations is needed to increase confidence in these results. Furthermore, this study is only able to examine the daily GPLLJ in a small number of models. Further research should examine the ability of the entire suite of CMIP5 models to simulate the diurnal cycle of the GPLLJ and the influence of ENSO on the frequency and intensity of daily GPLLJ events.

The CMIP5 models suffer from many limitations and biases as well, and future studies should examine the impact of these limitations on the models' ability to simulate features and mechanisms of the GPLLJ. As shown by Table 1, they have relatively coarse horizontal resolutions, which is likely causing many topographical features to be poorly represented. This could be inhibiting the models' ability to simulate orographic mechanisms of the GPLLJ, such as those proposed by Wexler (1961) and Holton (1967). Additional research should investigate whether models with higher resolutions are more capable of capturing the observed features and mechanisms of the GPLLJ. This could be done by running a climate model experiment that changes just the resolution of the model and then examines how the accuracy of GPLLJ characteristics, such as its strength, timing, vertical structure, and relationship with ENSO, may have changed. Furthermore, while this study found some reasons for the inability of the CMIP5 models to simulate the observed relationship between ENSO and the GPLLJ, other factors could be in play as well. For example, a narrow bias in ENSO meridional width has been found in the CMIP5 models, in this study and in past studies (Zhang and Jin 2012). Krishnamurthy et al. (2015) discovered too much ENSO variability and inaccurate phase locking in the GFDL FLOR coupled climate model. Further studies should analyze how much the failure of CMIP5 models to accurately represent the ENSO - GPLLJ relationship can be attributed to these and other biases, and how these errors can be reduced in future generations of climate models.

While this study mainly focused on the role of ENSO in driving the variability of the GPLLJ, it is clear from previous studies and from Appendix C that other teleconnections are important as well. Harding and Snyder (2015) discovered that a

negative PNA phase drives a stronger GPLLJ, which is confirmed by Figs. C1a-c and C2a-c. The CMIP5 model mean is able to capture this relationship as well (Figs. C1d and C2d). However, the models with the worst depiction of the DJF ENSO – MAM GPLLJ correlation (Fig. C1f) do not simulate the wave train in the Pacific that is seen in the other models and in the reanalyzes, which indicates that this may be playing a role in the inability of some models to capture the accurate ENSO - GPLLJ relationship in the spring. It has also been found that a negative PDO pattern drives a stronger springtime GPLLJ (Muñoz and Enfield 2011), which is consistent with the reanalyzes in Figs. C3a-c. In addition, the MAM GPLLJ is enhanced by a dipole between warm SSTs in the GOM and cold SSTs in the Caribbean Sea (Figs. C3a-c). The CMIP5 model mean successfully simulates the pattern of these SST influences on the MAM GPLLJ, but the correlations are weaker than in the reanalyzes, and the meridional width of the ENSO influence is too narrow (Fig. C3d). Furthermore, these influences are far too weak in the models with the least negative DJF ENSO – MAM GPLLJ correlation (Fig. C3f). In JAS, the PDO phase associated with a stronger GPLLJ flips to positive in the reanalyzes (Figs. C4a-c), while it stays weakly negative in the CMIP5 model mean (Fig. C4d). Lastly, the importance of the CLLJ in driving a stronger GPLLJ is evident in the reanalyzes (Figs. C5a-d; Figs. C6a-d) and in the models (Fig. C5e; Fig. C6e). Future work is needed to evaluate the ability of the CMIP5 models to capture these and other known mechanisms of the GPLLJ, in order to improve our ability to predict precipitation and severe weather over the Great Plains.

This study further developed our understanding of some of the most important features and mechanisms of the GPLLJ, particularly the relationship between the GPLLJ

58

and ENSO, in reanalyzes and CMIP5 models. Clearly, the ability of the CMIP5 models to simulate these features and mechanisms needs much improvement. It has been shown here that this can be partially attributed to a poor representation of the strength of ENSO and its impacts on the atmospheric circulation in the models. If these issues can be resolved, our ability to accurately predict and project the variability of the GPLLJ, and thus precipitation and severe weather over the Great Plains, will be greatly enhanced, which will be very beneficial for the livelihood of people living in the Great Plains.

References

Adachi, Y., and Coauthors, 2013: Basic performance of a new earth system model of the Meteorological Research Institute (MRI-ESM1). *Pap. Meteor. Geophys.*, **64**, 1–19, doi:10.2467/mripapers.64.1.

Arora, V. K., and Coauthors, 2011: Carbon emission limits required to satisfy future representative concentration pathways of greenhouse gases. *Geophys. Res. Lett.,* **38,** L05805, doi:10.1029/2010GL046270.

Arritt, R. W., T. D. Rink, M. Segal, D. P. Todey, C. A. Clark, M. J. Mitchell, and K. M. Labas, 1997: The Great Plains low-level jet during the warm season of 1993. *Mon. Wea. Rev.,* **125,** 2176–2192, doi:10.1175/1520-0493(1997)125<2176:TGPLLJ>2.0.CO;2.

Baek, H.-J., and Coauthors, 2013: Climate change in the 21st century simulated by HadGEM2-AO under representative concentration pathways. *Asia-Pac. J. Atmos. Sci.*, **49**, 603–618, doi:10.1007/s13143-013-0053-7.

Bao, Q., and Coauthors, 2012: The Flexible Global Ocean-Atmosphere-Land System model, spectral version 2: FGOALS-s2. *Adv. Atmos. Sci.,* **30,** 561–576, doi:10.1007/s00376-012-2113-9.

Barandiaran, D., S. Y. Wang, K. Hilburn, 2013: Observed trends in the Great Plains low-level jet and associated precipitation changes in relation to recent droughts. *Geophys. Res. Lett.,* **40,** 6247–6251, doi:10.1002/2013GL058296.

Bentsen, M., and Coauthors, 2013: The Norwegian Earth System Model, NorESM1-M—Part 1: Description and basic evaluation of the physical climate. *Geosci. Model Dev.*, **6**, 687–720, doi:10.5194/gmd-6-687-2013.

Berg, L. K., L. D. Riihimaki, Y. Qian, H. Yan, and M. Huang, 2015: The low-level jet over the southern Great Plains determined from observations and reanalyses and its impact on moisture transport. *J. Climate,* **28,** 6682–6706, doi:10.1175/JCLI-D-14-00719.1.

Blackadar, A. K., 1957: Boundary layer wind maxima and their significance for the growth of nocturnal inversions. *Bull. Amer. Meteor. Soc.,* **38,** 283–290.

Collins, M., S. F. B. Tett, and C. Cooper, 2001: The internal climate variability of HadCM3, a version of the Hadley Centre Coupled Model without flux adjustments. *Clim. Dyn.,* **17,** 61–81, doi:10.1007/s003820000094.

Compo, G. P., and Coauthors, 2011: The Twentieth Century Reanalysis project. *Quart. J. Roy. Meteor. Soc.,* **137,** 654, 1-28, doi:10.1002/qj.776.

Cook, K. H., E. K. Vizy, Z. S. Launer, and C. M. Patricola, 2008: Springtime intensification of the Great Plains low-level jet and Midwest precipitation in GCM simulations of the twenty-first century. *J. Climate,* **21,** 6321–6340, doi:10.1175/2008JCLI2355.1.

Cook, K. H., and E. K. Vizy, 2010: Hydrodynamics of the Caribbean low-level jet and its relationship to precipitation. *J. Climate,* **23,** 1477-1494, doi:10.1175/2009JCLI3210.1.

Delworth, T. L., and Coauthors, 2006: GFDL's CM2 global coupled climate models. Part I: Formulation and simulation characteristics. *J. Climate*, **19,** 643–674, doi:10.1175/JCLI3629.1.

Donner, L. J., and Coauthors, 2011: The dynamical core, physical parameterizations, and basic simulation characteristics of the atmospheric component AM3 of the GFDL global coupled model CM3. *J. Climate,* **24,** 3484–3519, doi:10.1175/2011JCLI3955.1.

Dufresne, J.-L., and Coauthors, 2013: Climate change projections using the IPSL-CM5 Earth System Model: from CMIP3 to CMIP5. *Clim. Dyn.,* **40**, 2123–2165, doi:10.1007/s00382-012-1636-1.

Eichler, T., and W. Higgins, 2006: Climatology and ENSO-related variability of North American extratropical cyclone activity. *J. Climate,* **19,** 2076-2093, doi:10.1175/JCLI3725.1.

Gent, P. R., and Coauthors, 2011: The Community Climate System Model version 4. *J. Climate,* **24,** 4973–4991, doi:10.1175/2011JCLI4083.1.

Harding, K. J.*,* and P. K. Snyder, 2014: Examining future changes in the character of Central U.S. warm-season precipitation using dynamical downscaling. *J. Geophys. Res. Atmos.*, **119,** 13,116–13,136*,* doi:10.1002/2014JD022575.

Harding, K. J., and P. K. Snyder, 2015: The relationship between the Pacific-North American Teleconnection Pattern, the Great Plains low-level jet, and North Central U.S. heavy rainfall events. *J. Climate,* **28,** 6729-6742, doi:10.1175/JCLI-D-14-00657.1.

Higgins, R. W., Y. Yao, E. S. Yarosh, J. E. Janowiak, and K. C. Mo, 1997: Influence of the Great Plains low-level jet on summertime precipitation and moisture transport over the central United States. *J. Climate,* **10,** 481–507, doi:10.1175/1520-0442(1997)010<0481:IOTGPL>2.0.CO;2.

Holton, J. R., 1967: The diurnal boundary layer wind oscillation above sloping terrain. *Tellus,* **19,** 199–205.

Huang, B., and Coauthors, 2015: Extended Reconstructed Sea Surface Temperature Version 4 (ERSST.v4). Part I: Upgrades and Intercomparisons. *J. Climate,* **28,** 911-930, doi:10.1175/JCLI-D-14-00006.1.

Hurwitz, M. M., N. Calvo, C. I. Garfinkel, A. H. Butler, S. Ineson, C. Cagnazzo, E. Manzini, C. Peña-Ortiz, 2014: Extra-tropical atmospheric response to ENSO in the CMIP5 models. *Clim. Dyn.,* **43,** 3367-3376, doi:10.1007/s00382-014-2110-z.

Jiang, X., N.-C. Lau, I. M. Held, and J. J. Ploshay, 2007: Mechanisms of the Great Plains low-level jet as simulated in an AGCM. *J. Atmos. Sci.,* **64,** 532-547, doi:10.1175/JAS3847.1.

Jones, C. D., and Coauthors, 2011: The HadGEM2-ES implementation of CMIP5 centennial simulations. *Geosci. Model Dev.,* **4,** 543–570, doi:10.5194/gmd-4-543-2011.

Kim, D., A. H. Sobel, A. D. Del Genio, Y. Chen, S. J. Camargo, M.-S. Yao, M. Kelley, and L. Nazarenko, 2012: The tropical subseasonal variability simulated in the NASA GISS general circulation model. *J. Climate*, **25**, 4641–4659, doi:10.1175/JCLI-D-11-00447.1.

Kim, S. T., and J.-Y. Yu, 2012: The two types of ENSO in CMIP5 models. *Geophys. Res. Lett.,* **39,** L11704, doi:10.1029/2012GL052006.

Krishnamurthy, L., G. A. Vecchi, R. Msadek, A. Wittenberg, T. L. Delworth, and F. Zeng, 2015: The seasonality of the Great Plains low-level jet and ENSO relationship. *J. Climate,* **28,** 4525-4544, doi:10.1175/JCLI-D-14-00590.1.

Lee, S. K., R. Atlas, D. Enfield, C. Wang, and H. Liu, 2013: Is there an optimal ENSO pattern that enhances large-scale atmospheric processes conducive to tornado outbreaks in the United States?. *J. Climate,* **26,** 1626–1642, doi:10.1175/JCLI-D-12-00128.1.

Li, L., and Coauthors, 2013: The flexible global ocean–atmosphere–land system model, grid-point version 2: FGOALS-g2. *Adv. Atmos. Sci.*, **30**, 543–560, doi:10.1007/s00376-012-2140-6.

Liang, Y.-C., J.-Y. Yu, M.-H. Lo, and C. Wang, 2015: The changing influence of El Niño on the Great Plains low-level jet. *Atmos. Sci. Lett.,* **16,** 512-517, doi:10.1002/asl.590.

Long, M. C., K. Lindsay, S. Peacock, J. K. Moore, and S. C. Doney, 2013: Twentieth-century oceanic carbon uptake and storage in CESM1(BGC). *J. Climate*, **26**, 6775–6800, doi:10.1175/JCLI-D-12-00184.1.

Martin, E. R., and C. Schumacher, 2011: The Caribbean low-level jet and its relationship with precipitation in IPCC AR4 models. *J. Climate,* **24,** 5935-5950, doi:10.1175/JCLI-D-11-00134.1.

Marsh, D. R., M. J. Mills, D. E. Kinnison, J.-F. Lamarque, N. Calvo, and L. M. Polvani, 2013: Climate change from 1850 to 2005 simulated in CESM1(WACCM). *J. Climate*, **26**, 7372–7391, doi:10.1175/JCLI-D-12-00558.1.

Meehl, G. A., and Coauthors, 2013: Climate change projections in CESM1(CAM5) compared to CCSM4. *J. Climate*, **26**, 6287–6308, doi:10.1175/JCLI-D-12-00572.1.

Muñoz, E., and D. Enfield, 2011: The boreal spring variability of the Intra-Americas low-level jet and its relation with precipitation and tornadoes in the eastern United States. *Clim. Dyn.,* **36,** 247–259, doi:10.1007/s00382-009-0688-3.

Perez, J., M. Menendez, F. J. Mendez, and I. J. Losada, 2014: Evaluating the performance of CMIP3 and CMIP5 global climate models over the north-east Atlantic region. *Clim. Dyn.,* **43,** 2663-2680, doi:10.1007/s00382-014-2078-8.

Phipps, S. J., L. D. Rotstayn, H. B. Gordon, J. L. Roberts, A. C. Hirst, and W. F. Budd, 2011: The CSIRO Mk3L climate system model version 1.0—Part 1: Description and evaluation. *Geosci. Model Dev.*, **4**, 483–509, doi:10.5194/gmd-4-483-2011.

Polade, S. D.*,* A. Gershunov, D. R. Cayan, M. D. Dettinger, and D. W. Pierce, 2013: Natural climate variability and teleconnections to precipitation over the Pacific-North American region in CMIP3 and CMIP5 models. *Geophys. Res. Lett.,* **40,** 2296–2301, doi:10.1002/grl.50491.

Poli, P., and Coauthors, 2016: ERA-20C: An atmospheric reanalysis of the twentieth century. *J. Climate,* **29,** 4083-4097, doi:10.1175/JCLI-D-15-0556.1.

Pu, B., and R. E. Dickinson, 2014: Diurnal spatial variability of Great Plains summer precipitation related to the dynamics of the low-level jet. *J. Atmos. Sci.,* **71,** 1807-1817, doi:10.1175/JAS-D-13-0243.1.

Rayner, N. A.*,* D. E. Parker*,* E. B. Horton*,* C. K. Folland*,* L. V. Alexander*,* D. P. Rowell*,* E. C. Kent*,* and A. Kaplan*,* 2003: Global analyses of sea surface temperature, sea ice, and night marine air temperature since the late nineteenth century. *J. Geophys. Res.,* **108,** D14, 4407, doi:10.1029/2002JD002670.

Saha, S., and Coauthors, 2010: The NCEP Climate Forecast System Reanalysis. *Bull. Amer. Meteor. Soc.,* **91**, 1015–1057, doi:10.1175/2010BAMS3001.1.

Schubert, S., M. J. Suarez, P. J. Pegion, R. D. Koster, and J. T. Bacmeister, 2004: Causes of long-term drought in the U.S. Great Plains. *J. Climate,* **17,** 485–503, doi:10.1175/1520-0442(2004)017<0485:COLDIT>2.0.CO;2.

Sheffield, J., and Coauthors, 2013: North American climate in CMIP5 experiments. Part I: evaluation of historical simulations of continental and regional climatology. *J. Climate,* **26**, 9209–9245, doi:10.1175/JCLI-D-12-00592.1.

Shinker, J. J., and P. J. Bartlein, 2009: Visualizing the large-scale patterns of ENSO-related climate anomalies in North America. *Earth Interactions,* **13,** 3, 1-50, doi: 10.1175/2008EI244.1.

Simmons, A. J., P. Poli, D. P. Dee, P. Berrisford, H. Hersbach, S. Kobayashi, and C. Peubey, 2014: Estimating low-frequency variability and trends in atmospheric temperature using ERA-Interim. *Quart. J. Roy. Meteor. Soc.,* **140,** 679, 329-353, doi:10.1002/qj.2317.

Stensrud, D. J., 1996: Importance of low-level jets to climate: a review. *J. Climate,* **9,** 1698-1711, doi:10.1175/1520-0442(1996)009<1698:IOLLJT>2.0.CO;2.

Trenberth, K. E., and C. J. Guillemot, 1996: Physical processes involved in the 1988 drought and 1993 floods in North America. *J. Climate,* **9,** 1288–1298, doi:10.1175/1520-0442(1996)009<1288:PPIITD>2.0.CO;2.

Uccellini, L. W., 1980: On the role of upper tropospheric jet streaks and leeside cyclogenesis in the development of low-level jets in the Great Plains. *Mon. Wea. Rev.,* **108,** 1689-1696, doi:10.1175/1520-0493(1980)108<1689:OTROUT>2.0.CO;2.

Voldoire, A., and Coauthors, 2013: The CNRM-CM5.1 global climate model: Description and basic evaluation. *Clim. Dyn.,* **40,** 2091–2121, doi:10.1007/s00382-011-1259-y.

Volodin, E. M., N. A. Diansky, and A. V. Gusev, 2010: Simulating present-day climate with the INMCM4.0 coupled model of the atmospheric and oceanic general circulations. *Inv. Atmos. Oceanic Phys.,* **46,** 414–431, doi:10.1134/S000143381004002X.

Watanabe, M., and Coauthors, 2010: Improved climate simulation by MIROC5: Mean states, variability, and climate sensitivity. *J. Climate,* **23,** 6312–6335, doi:10.1175/2010JCLI3679.1.

Weaver, S. J., and S. Nigam, 2008: Variability of the Great Plains low-level jet: Large-scale circulation context and hydroclimate impacts. *J. Climate,* **21,** 1532-1551, doi:10.1175/2007JCLI1586.1.

Weaver, S. J., S. Schubert, and H. Wang, 2009: Warm season variations in the low-level circulation and precipitation over the central United States in observations, AMIP simulations, and idealized SST experiments. *J. Climate,* **22,** 5401–5420, doi:10.1175/2009JCLI2984.1.

Wexler, H., 1961: A boundary layer interpretation of the low level jet. *Tellus,* **13,** 368–378.

Xin, X., T. Wu, and J. Zhang, 2012: Introductions to the CMIP5 simulations conducted by the BCC climate system model (in Chinese). *Adv. Climate Change Res.,* **8,** 378–382.

Yukimoto, S., and Coauthors, 2012: A new global climate model of the Meteorological Research Institute: MRI-CGCM3—Model description and basic performance. *J. Meteor. Soc. Japan,* **90A,** 23–64, doi:10.2151/jmsj.2012-A02.

Zanchettin, D., A. Rubino, D. Matei, O. Bothe, and J. H. Jungclaus, 2013: Multidecadal-to-centennial SST variability in the MPI-ESM simulation ensemble for the last millennium. *Clim. Dyn.,* **40**, 1301-1318, doi:10.1007/s00382-012-1361-9.

Zhang, W., and F.-F. Jin, 2012: Improvements in the CMIP5 simulations of ENSO-SSTA meridional width, *Geophys. Res. Lett.,* **39,** L23704, doi:10.1029/2012GL053588.

Zhang, T., and D.-Z. Sun, 2014: ENSO asymmetry in CMIP5 models. *J. Climate,* **27,** 4070-4093, doi:10.1175/JCLI-D-13-00454.1.

Appendix A: Individual Model Statistics

Models	RMSE (m/s)
HadGEM2-AO	0.77
CanESM2	0.87
HadGEM2-ES	0.93
HadCM3	0.95
HadGEM2-CC	1.07
FGOALS-s2	1.27
CMCC-CESM	1.28
CESM1-WACCM	**1.39**
CNRM-CM5-2	1.46
MPI-ESM-LR	**1.46**
MPI-ESM-P	**1.47**
CSIRO-Mk3L-1-2	1.59
CNRM-CM5	1.62
CMCC-CMS	**1.63**
MPI-ESM-MR	**1.70**
bcc-csm1-1-m	1.77
CESM1-CAM5	**1.81**
GFDL-CM2.1	**1.87**
CMCC-CM	**2.05**
inmcm4	2.06
GFDL-CM3	**2.09**
GISS-E2-R-CC	**2.10**

CCSM4	**2.15**
GISS-E2-R	**2.16**
CESM1-FASTCHEM	**2.17**
MIROC5	**2.23**
GISS-E2-H-CC	**2.23**
CESM1-BGC	**2.28**
bcc-csm1-1	**2.28**
GFDL-ESM2G	**2.29**
IPSL-CM5A-MR	**2.32**
MRI-CGCM3	2.34
NorESM1-ME	**2.34**
NorESM1-M	**2.34**
GFDL-ESM2M	**2.35**
MRI-ESM1	2.37
GISS-E2-H	**2.40**
FGOALS-g2	2.46
IPSL-CM5A-LR	**2.82**
IPSL-CM5B-LR	**2.92**
MIROC-ESM	2.99
MIROC-ESM-CHEM	3.01
Model Mean	**1.87**

Table A1: The root mean squared error between the MAM GPLLJ in each CMIP5 model and the MAM GPLLJ in the 20CR. The models are ranked from least to greatest RMSE. The model name and RMSE are bolded and shaded blue if the 95% confidence interval of the bootstrapped differences (R=1000) for the model is entirely negative, and they are bolded and shaded red if the 95% confidence interval is entirely positive.

Models	RMSE (m/s)
CESM1-CAM5	0.42
MPI-ESM-LR	0.44
CMCC-CM	0.45
HadCM3	0.48
MPI-ESM-P	0.51
GFDL-CM2.1	0.53
CNRM-CM5	0.56
CNRM-CM5-2	0.58
MIROC5	0.59
CMCC-CMS	0.59
MPI-ESM-MR	0.68
CESM1-BGC	0.74
CCSM4	0.74
NorESM1-ME	0.76
CESM1-WACCM	0.79
bcc-csm1-1-m	0.81
CESM1-FASTCHEM	0.82
NorESM1-M	0.85
GFDL-ESM2M	0.90
CSIRO-Mk3L-1-2	1.05
CanESM2	1.05
GFDL-ESM2G	**1.10**
bcc-csm1-1	1.11

HadGEM2-AO	**1.18**
MRI-CGCM3	1.31
FGOALS-g2	1.32
MRI-ESM1	1.32
CMCC-CESM	1.44
HadGEM2-ES	1.46
inmcm4	1.46
GFDL-CM3	**1.49**
MIROC-ESM	1.51
HadGEM2-CC	**1.52**
MIROC-ESM-CHEM	1.53
IPSL-CM5A-MR	1.58
IPSL-CM5A-LR	1.80
FGOALS-s2	**1.82**
IPSL-CM5B-LR	1.88
GISS-E2-R-CC	**2.11**
GISS-E2-H	**2.14**
GISS-E2-H-CC	**2.21**
GISS-E2-R	**2.23**
Model Mean	0.48

Table A2: Same as Table A1, but for the JAS GPLLJ.

Models	DJF ENSO – MAM GPLLJ correlation
CCSM4	-0.501
CMCC-CMS	-0.445
CESM1-BGC	-0.444
CESM1-FASTCHEM	-0.415
CNRM-CM5-2	-0.410
CESM1-CAM5	-0.402
GFDL-CM2.1	-0.388
bcc-csm1-1-m	-0.379
NorESM1-ME	-0.377
GFDL-ESM2M	-0.375
CESM1-WACCM	-0.361
GISS-E2-R-CC	-0.359
GFDL-CM3	-0.352
CanESM2	-0.324
CNRM-CM5	-0.321
NorESM1-M	-0.304
FGOALS-s2	-0.292
MRI-CGCM3	-0.286
CMCC-CESM	-0.275
MIROC5	-0.229
IPSL-CM5B-LR	-0.225
CSIRO-Mk3L-1-2	-0.220
MPI-ESM-MR	-0.212

HadGEM2-ES	**-0.211**
GFDL-ESM2G	**-0.210**
IPSL-CM5A-LR	**-0.206**
IPSL-CM5A-MR	-0.179
GISS-E2-H-CC	-0.177
HadGEM2-AO	-0.175
HadGEM2-CC	-0.174
MPI-ESM-LR	-0.151
MRI-ESM1	-0.147
HadCM3	-0.146
FGOALS-g2	-0.129
CMCC-CM	-0.093
bcc-csm1-1	-0.067
GISS-E2-R	-0.065
MPI-ESM-P	-0.041
GISS-E2-H	-0.035
inmcm4	0.006
MIROC-ESM-CHEM	0.054
MIROC-ESM	0.139

Table A3: The correlation between DJF ENSO and the following MAM GPLLJ anomaly in each CMIP5 model. Statistically significant negative correlations at the 95% level (along with the corresponding model name) are bolded and shaded blue, and significant positive correlations (along with the corresponding model name) are bolded and shaded red.

Models	DJF ENSO – JAS GPLLJ correlation
CMCC-CMS	0.112
bcc-csm1-1	0.094
CNRM-CM5-2	0.056
HadGEM2-AO	0.050
FGOALS-s2	0.047
GISS-E2-R	0.026
MRI-CGCM3	0.024
bcc-csm1-1-m	0.023
FGOALS-g2	0.013
CanESM2	0.008
CMCC-CESM	0.006
MPI-ESM-P	0.005
GISS-E2-H	-0.001
HadGEM2-ES	-0.006
GISS-E2-R-CC	-0.011
CNRM-CM5	-0.014
CMCC-CM	-0.024
HadCM3	-0.030
MIROC-ESM	-0.034
CSIRO-Mk3L-1-2	-0.053
MIROC-ESM-CHEM	-0.056
MPI-ESM-LR	-0.072
MPI-ESM-MR	-0.074

CESM1-CAM5	-0.107
GFDL-ESM2G	-0.107
IPSL-CM5A-LR	-0.113
IPSL-CM5A-MR	-0.121
HadGEM2-CC	-0.132
GFDL-CM3	-0.132
MRI-ESM1	-0.137
MIROC5	-0.151
NorESM1-ME	-0.163
CCSM4	-0.173
IPSL-CM5B-LR	**-0.193**
NorESM1-M	**-0.197**
CESM1-WACCM	**-0.211**
inmcm4	**-0.229**
CESM1-BGC	**-0.246**
GFDL-ESM2M	**-0.268**
CESM1-FASTCHEM	**-0.272**
GISS-E2-H-CC	**-0.283**
GFDL-CM2.1	**-0.316**

Table A4: Same as Table A3, but for the correlation between DJF ENSO and the following JAS GPLLJ.

Appendix B: Additional Information on Best and Worst Models
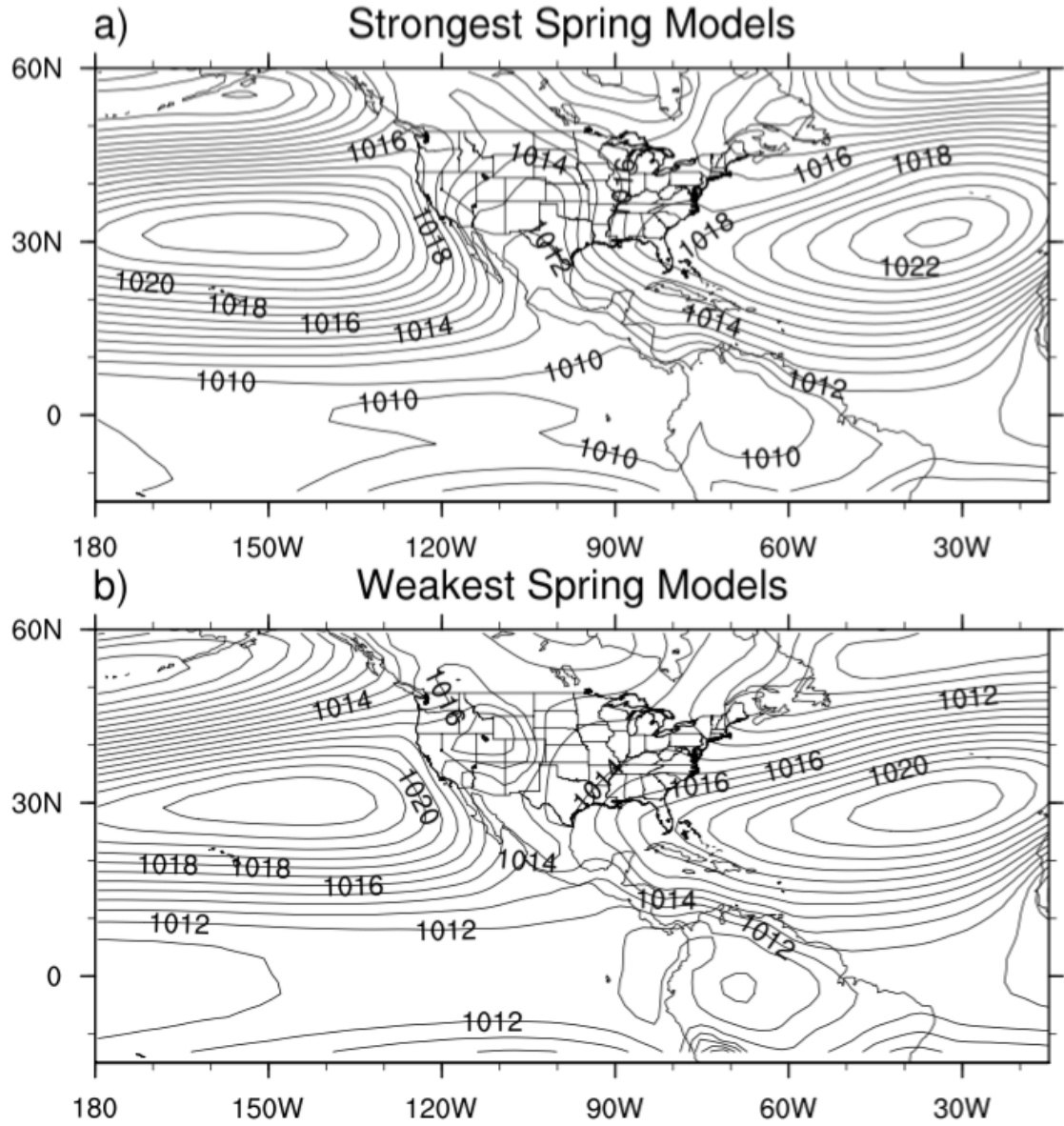
Fig. B1: Mean MAM SLP (hPa) in the "strongest spring models" (a) and the "weakest spring models" (b).
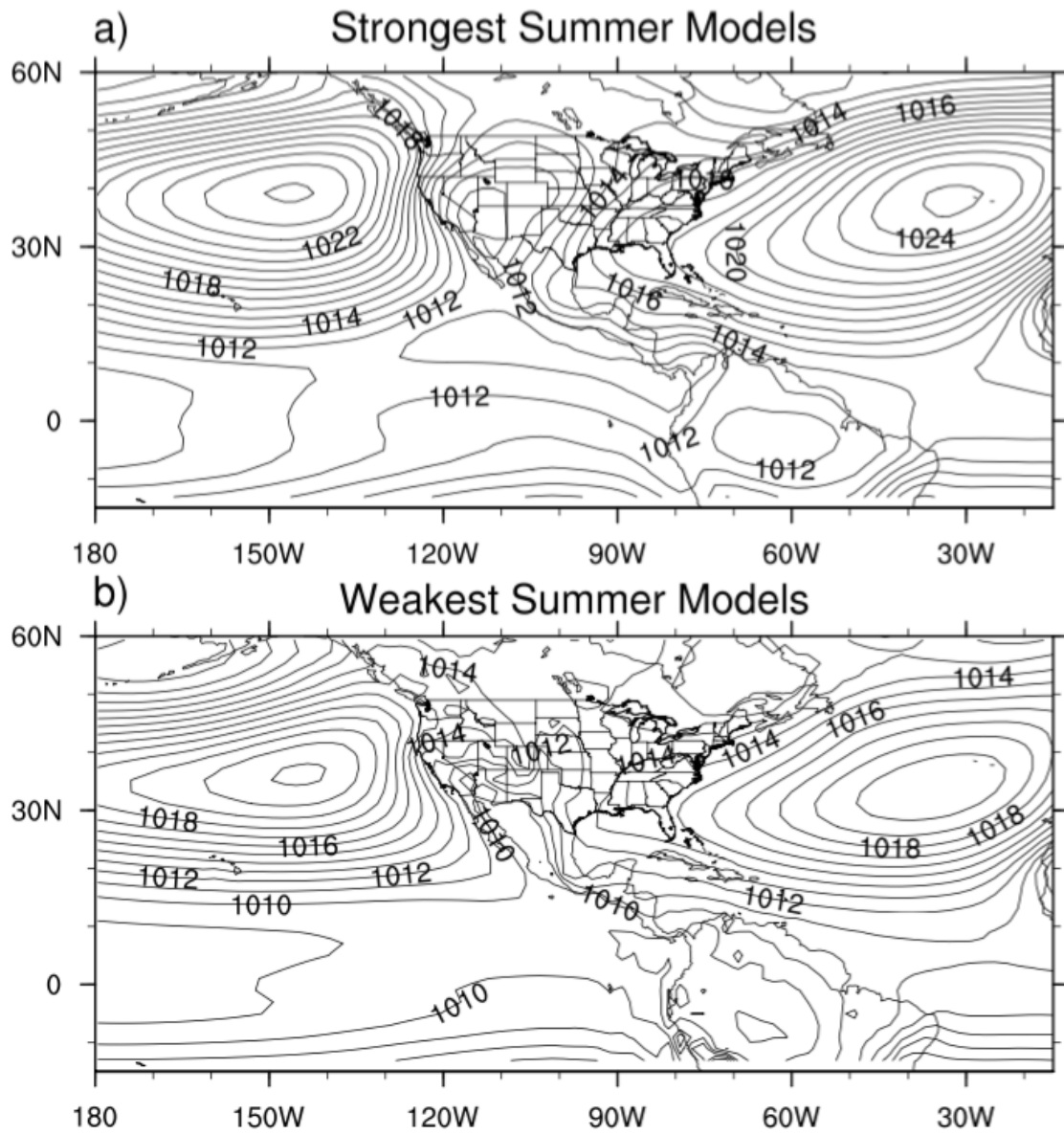
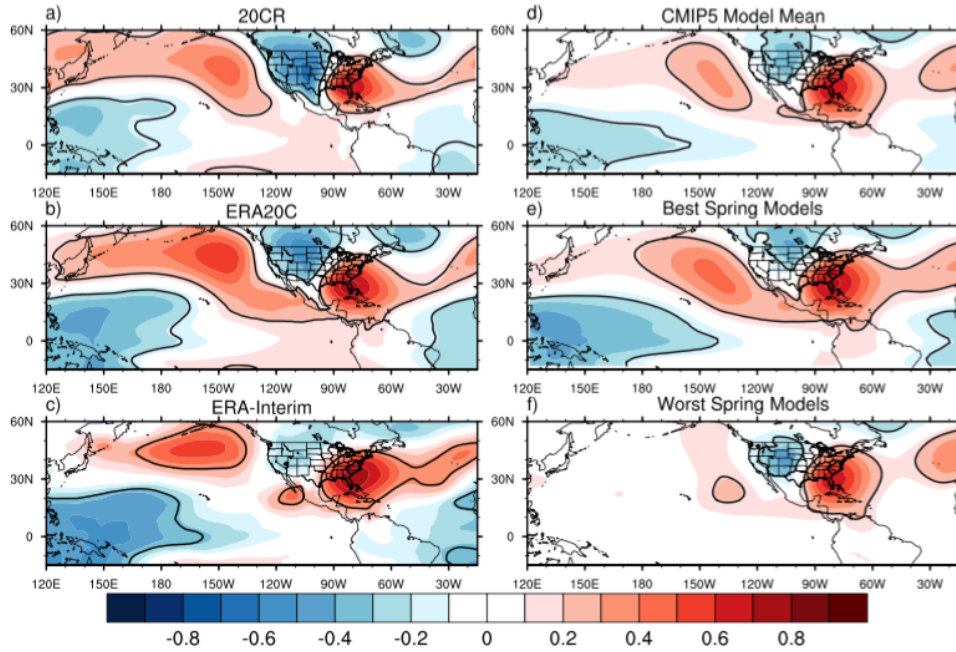**Fig. B2: Mean JAS SLP (hPa) in the "strongest summer models" (a) and the "weakest summer models" (b).**
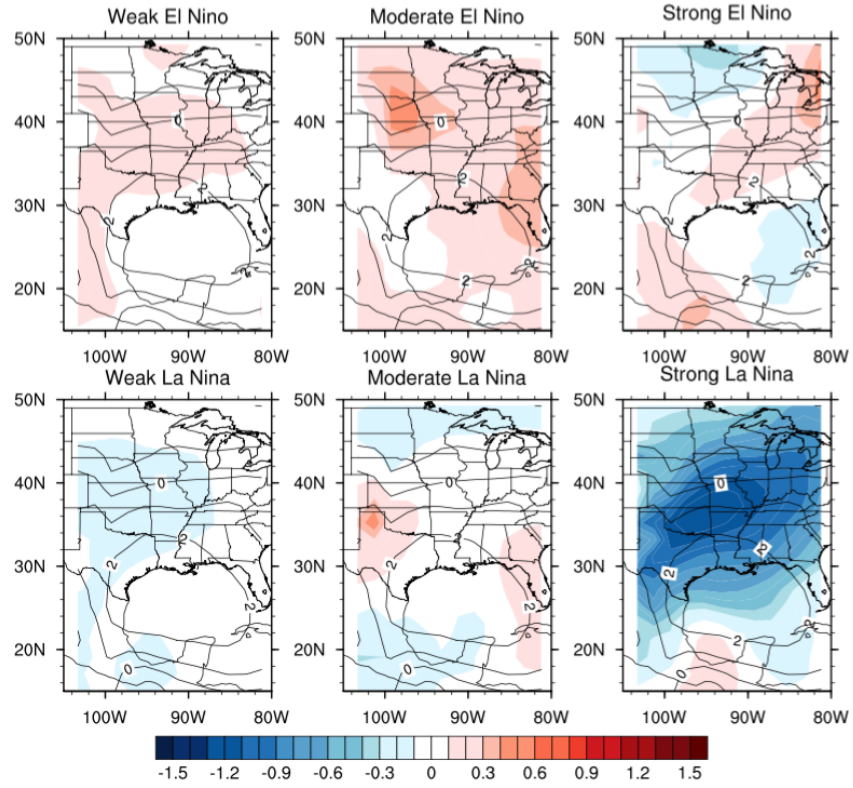
**Fig. B3: Same as Fig. 15, but for the "worst spring models".**
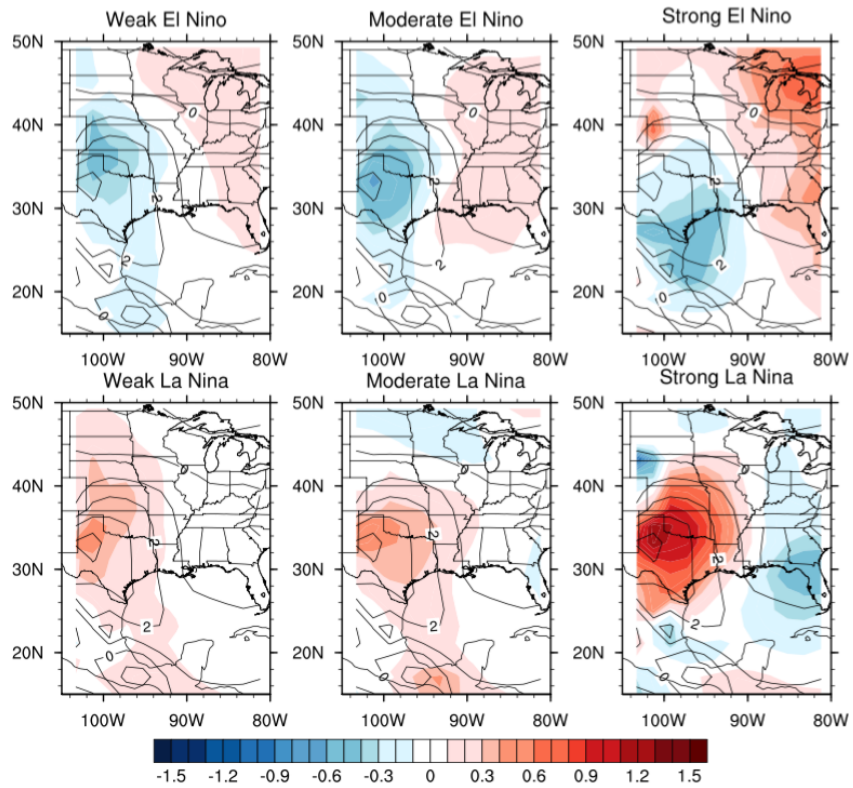
**Fig. B4: Same as Fig. 16, but for the "worst summer models".**
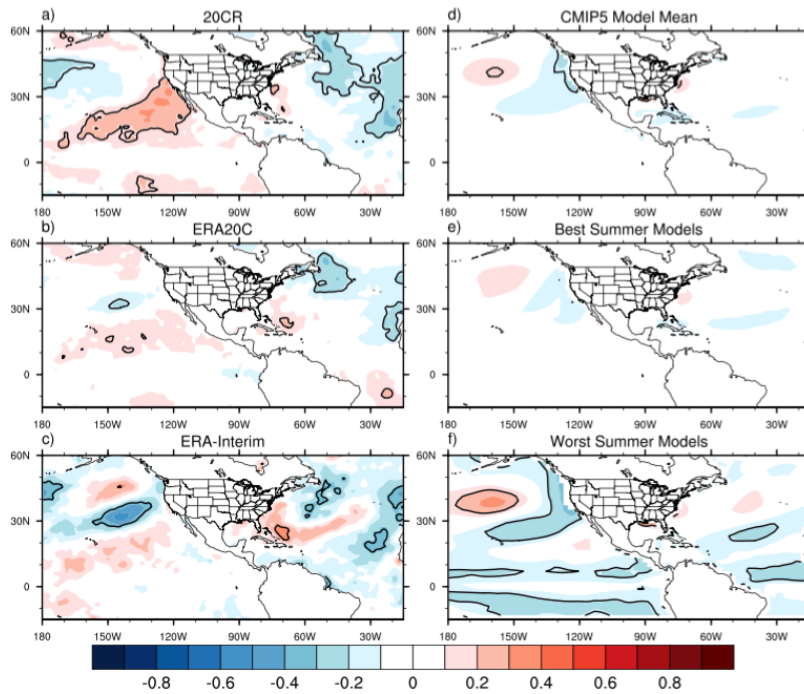
Appendix C: Other Mechanisms of the GPLLJ

Fig. C1: Instantaneous correlation between GPLLJ anomalies and 850-hPa geopotential height anomalies in MAM in the 20CR (a), ERA20C (b), ERA-Interim (c), CMIP5 model mean (d), "best spring models" (e), and "worst spring models" (f). All correlations within the bolded line are statistically significant at the 95% confidence level using a two-tailed probability test.
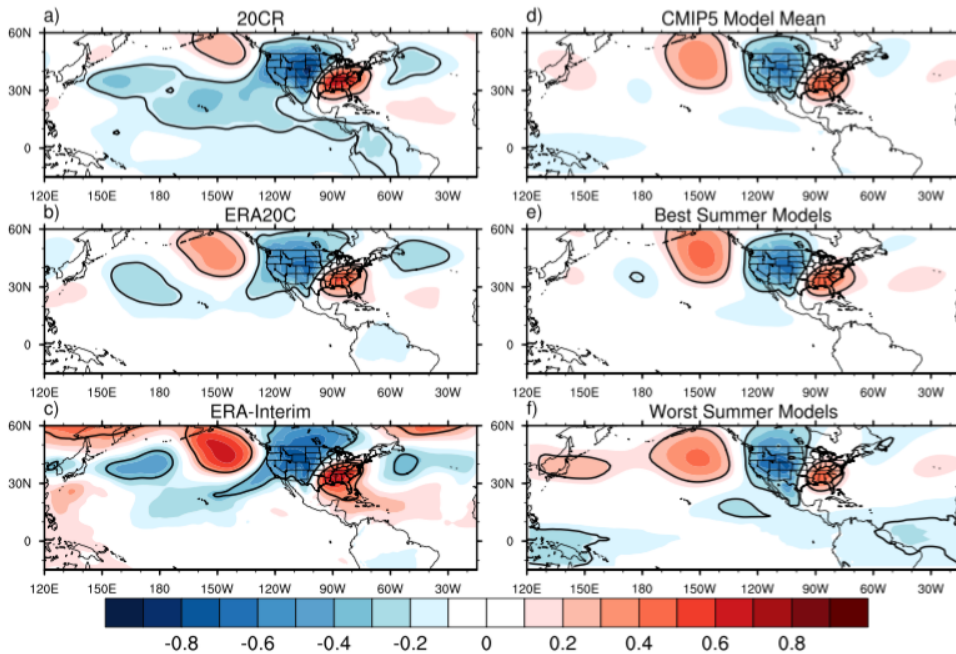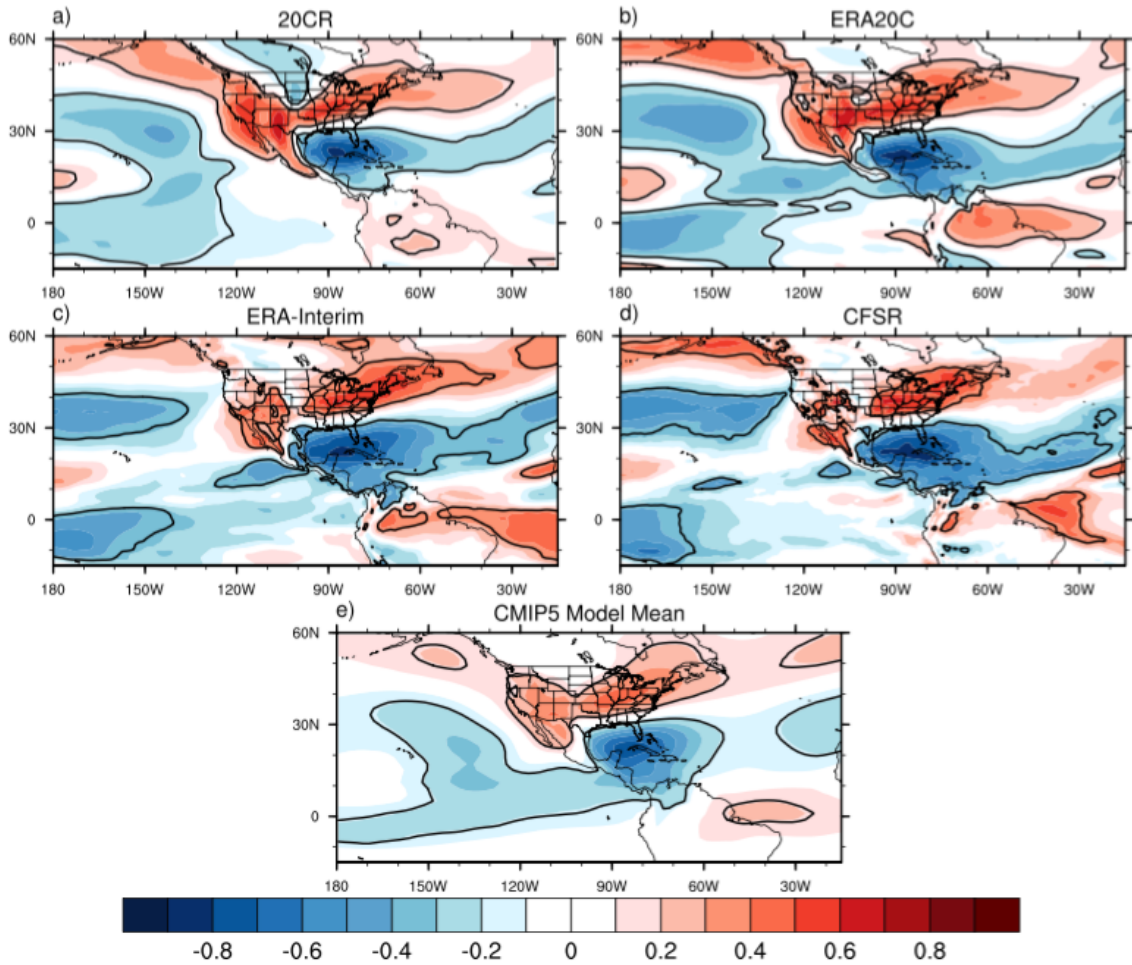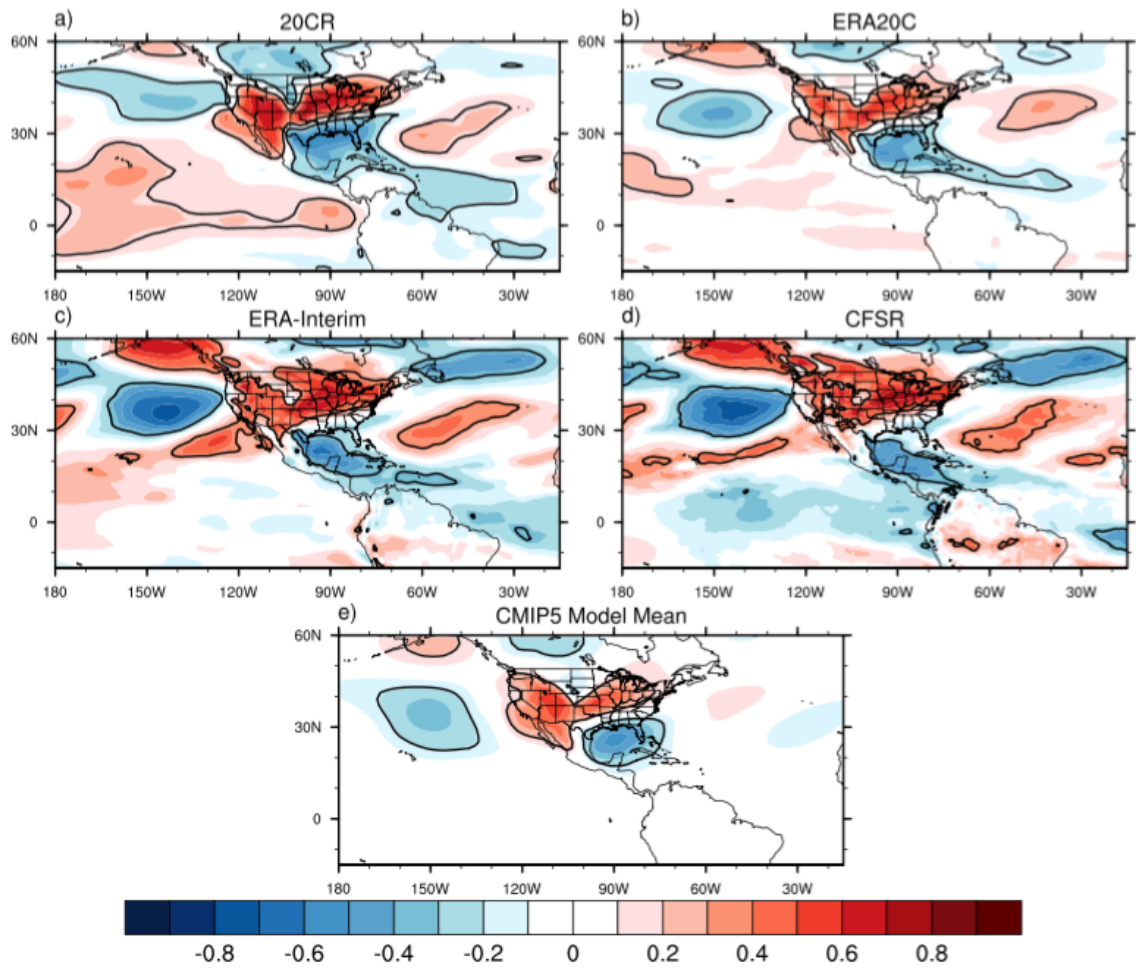

Fig. C2: Same as Fig. C1, but for JAS.
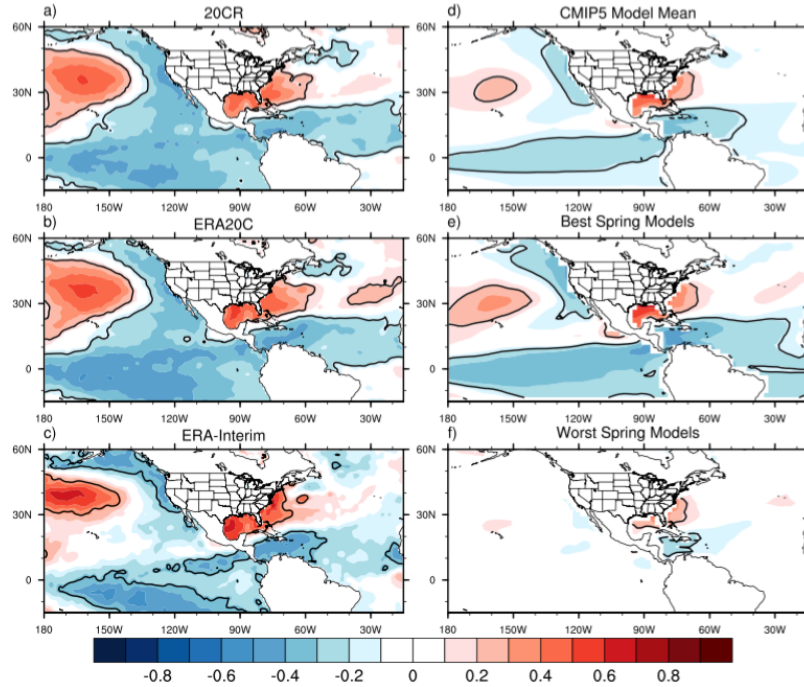
Fig. C3: Instantaneous correlation between GPLLJ anomalies and SST anomalies in MAM in the 20CR (a), ERA20C (b), ERA-Interim (c), CMIP5 model mean (d), "best spring models" (e), and "worst spring models" (f). All correlations within the bolded line are statistically significant at the 95% confidence level using a two-tailed probability test.

Fig. C4: Same as Fig. C3, but for JAS.

Fig. C5: Instantaneous correlation between GPLLJ anomalies and zonal wind anomalies in MAM in the 20CR (a), ERA20C (b), ERA-Interim (c), CFSR (d), and CMIP5 model mean (e). All correlations within the bolded line are statistically significant at the 95% confidence level using a two-tailed probability test.

Fig. C6: Same as Fig. C5, but for JAS.